



Modeling brine and nutrient dynamics in Antarctic sea ice: The case of dissolved silica

Martin Vancoppenolle,¹ Hugues Goosse,¹ Anne de Montety,¹ Thierry Fichet,¹
Bruno Tremblay,² and Jean-Louis Tison³

Received 9 March 2009; revised 14 September 2009; accepted 15 October 2009; published 4 February 2010.

[1] Sea ice ecosystems are characterized by microalgae living in brine inclusions. The growth rate of ice algae depends on light and nutrient supply. Here, the interactions between nutrients and brine dynamics under the influence of algae are investigated using a one-dimensional model. The model includes snow and ice thermodynamics with brine physics and an idealized sea ice biological component, characterized by one nutrient, namely, dissolved silica (DSi). In the model, DSi follows brine motion and is consumed by ice algae. Depending on physical ice characteristics, the brine flow is either advective, diffusive, or turbulent. The vertical profiles of ice salinity and DSi concentration are solutions of advection-diffusion equations. The model is configured to simulate the typical thermodynamic regimes of first-year Antarctic pack ice. The simulated vertical profiles of salinity and DSi qualitatively reproduce observations. Analysis of results highlights the role of convection in the lowermost 5–10 cm of ice. Convection mixes saline, nutrient-poor brine with comparatively fresh, nutrient-rich seawater. This implies a rejection of salt to the ocean and a flux of DSi to the ice. In the presence of growing algae, the simulated ocean-to-ice DSi flux increases by 0–115% compared to an abiotic situation. In turn, primary production and brine convection act in synergy to form a nutrient pump. The other important processes are the flooding of the surface by seawater and the percolation of meltwater. The former refills nutrients near the ice surface in spring. The latter, if present, tends to expell nutrients from the ice in summer.

Citation: Vancoppenolle, M., H. Goosse, A. de Montety, T. Fichet, B. Tremblay, and J.-L. Tison (2010), Modeling brine and nutrient dynamics in Antarctic sea ice: The case of dissolved silica, *J. Geophys. Res.*, 115, C02005, doi:10.1029/2009JC005369.

1. Introduction

[2] While many studies were dedicated to the role of sea ice in the climate system by means of direct physical interactions [e.g., Holland *et al.*, 2006; Serreze *et al.*, 2007], the interactions between sea ice and the main biogeochemical cycles were comparatively less investigated. Yet sea ice is one of the largest Earth biomes, which hosts a complex web of microorganisms consuming and producing biogases with a potential climate impact [Thomas and Dieckmann, 2003]. For instance, sea ice affects the atmosphere-ocean CO₂ exchanges in a complex way because of a highly variable permeability, specific carbonate chemistry, and algal growth within the ice [Semiletov *et al.*, 2004; Delille, 2006]. Sea ice is also laden with large iron stocks [Lannuzel *et al.*, 2007, 2008], which, when released

during summer melt, stimulate summer phytoplankton blooms in the vicinity of the Antarctic marginal ice zones [Lancelot *et al.*, 2009].

[3] In spring and summer, sea ice may appear green or brown because of ice algae living in the liquid brine inclusions [Krems *et al.*, 2002]. Ice algae are adapted to life in extreme salt and temperature conditions [Thomas and Dieckmann, 2003] and can be limited by either light or nutrients [e.g., Arrigo *et al.*, 1993; Lavoie *et al.*, 2005]. Sea ice communities typically develop near the surface and the base of the ice cover [Ackley and Sullivan, 1994]. As the observed nutrient stocks in sea ice are not large enough to explain primary production estimates [e.g., Kottmeier and Sullivan, 1987], nutrient supply to the sea ice communities is required to sustain algal growth. However, the mechanisms for nutrient supply in sea ice are currently poorly understood and quantified.

[4] The sea ice crystalline lattice hardly tolerates impurities. In practice, one can consider that all salts and nutrients are dissolved in brine. The pure ice itself is nearly salt- and nutrient-free. Brine inclusions are dynamic and their size depends on the sea ice temperature and bulk salinity (i.e., salinity of pure ice plus brine) [see, e.g., Light *et al.*, 2003]. For brine volume fractions above ~5%, the brine pockets coalesce and form brine channels [Eide and Martin, 1975;

¹Institut d'Astronomie et de Géophysique Georges Lemaître, Université Catholique de Louvain, Louvain-la-Neuve, Belgium.

²Department of Atmospheric and Oceanic Sciences, McGill University, Montreal, Quebec, Canada.

³Laboratoire de Glaciologie, Université Libre de Bruxelles, Brussels, Belgium.

Golden *et al.*, 1998]. Near the ice base, brine channels provide open pathways for brine drainage and material exchange between ice and ocean.

[5] Brine drainage, which induces a net desalination of the ice over time, is controlled by two mechanisms, namely gravity drainage and flushing [Untersteiner, 1968; Vancoppenolle *et al.*, 2006; Notz and Worster, 2009]. Gravity drainage is the convective overturning of brine in connected inclusions. [Cox and Weeks, 1975; Notz and Worster, 2008]. During cold periods, the temperature decreases upward. Brine salinity increases at low temperatures; hence, brine salinity and density increase upward, which destabilizes the brine column. Convection was directly observed during laboratory experiments, in both the highly porous interfacial zone between ice and ocean “skeletal layer”) and the connected brine channels just above [Niedrauer and Martin, 1979]. Brine overturning over the whole ice thickness has also been suggested to follow the flooding of the ice surface by seawater [Lytle and Ackley, 1996; Maksym and Jeffries, 2000]. The second desalination mechanism, flushing, refers to the percolation of fresh meltwater through the permeable brine network. Meltwater replaces saline brine [Eicken *et al.*, 2002; Vancoppenolle *et al.*, 2007], which intensely freshens sea ice in summer.

[6] It has been hypothesized that brine dynamics control dissolved nutrient supply to the sea ice communities [Reeburgh, 1984], for two reasons. First, brine convection in the skeletal layer seems intense enough to provide the required nutrients to sustain primary production. Second, the vertical profiles of dissolved macronutrient concentrations and salinity within the ice have similar shape, as indicated by field and laboratory experiments [Clarke and Ackley, 1984; Cota *et al.*, 1987; Giannelli *et al.*, 2001; Tison *et al.*, 2008]. However, this brine hypothesis for nutrient supply has never been tested quantitatively. Given the relatively poor understanding of brine dynamics, the nutrient fluxes in sea ice model are either prescribed [e.g., Arrigo *et al.*, 1993; Fritsen *et al.*, 1998] or formulated using various prescribed diffusivity values [e.g., Lavoie *et al.*, 2005; Nishi and Tabeta, 2008]. Recently, brine dynamics have been introduced in some sea ice models [Notz and Worster, 2006; Vancoppenolle *et al.*, 2007], which enables a more realistic representation of nutrients.

[7] In this paper, we test the hypothesis that brine dynamics provide nutrient supply using a one-dimensional biophysical sea ice model. We focus on dissolved silica (DSi) in Antarctic pack ice (section 2) and specifically investigate the role of convection, algal uptake, and snowfall rate on DSi. In addition, the biophysical interactions (i.e., those between brine dynamics and nutrients under the influence of primary production) are analyzed. The model (see section 3) includes snow and ice thermodynamics with explicit brine physics and an idealized sea ice biological component. The latter is characterized by a single dissolved macronutrient, namely, DSi. DSi stocks are reduced by algal uptake computed using a prescribed rate of primary production. The biological component of the model is deliberately kept simple in order to highlight biophysical interactions. The model is configured in an idealized setup (section 4) designed to simulate the typical evolution of undeformed first-year Antarctic pack ice. In section 5, we compare the simulated salinity and DSi profiles and fluxes to various

observations. In order to get insight into the physics of brine drainage, the sensitivity of the results to several model parameters is investigated. Intense convective events and biophysical interactions are also specifically analyzed. The results are discussed in section 6 and conclusions are given in section 7.

2. Antarctic Sea Ice Characteristics

[8] The focus of this paper is on undeformed first-year pack ice (0–1.5 m), which is the most abundant ice type in the Antarctic sea ice cover [Worby *et al.*, 2008]. This ice type is typically a mixture of columnar ice [Gow *et al.*, 1987; Haas *et al.*, 2008; Tison *et al.*, 2008] and granular ice of frazil origin [Lange and Eicken, 1991; Jeffries *et al.*, 1994; Worby and R. A. Massom, 1995]. Granular ice is particularly present in thin ice (<40 cm) and thick deformed ice [Gow *et al.*, 1987]. Here we do not consider frazil ice formation.

[9] One of the key features of the Antarctic sea ice pack is the deep snow cover [see, e.g., Massom *et al.*, 2001]. Typically, snow depth lies within the range 0–30 cm. However, in some regions, like in the coastal Amundsen and Bellingshausen Seas, large snowfall rates lead to mean snow depths of 60 cm on average and may reach more than 1 m [Worby *et al.*, 2008]. In spring, deep snow leads to negative freeboards and snow ice formation. Snow ice constitutes up to 24% of the total sea ice mass in this region [Jeffries *et al.*, 1997].

[10] All Antarctic sea ice algae rely on nitrate and phosphate for growth. In addition, diatoms also require silica to build up their cell walls. Antarctic sea ice algal basal communities are highly dominated by those diatoms [Lizotte, 2003], while surface communities (less frequent) typically consist of *Phaeocystis sp.* DSi is thus an essential component of their metabolism and was reported as potentially limiting in Antarctic sea ice [e.g., Thomas and Papadimitriou, 2003; Fripiat *et al.*, 2007]. DSi is therefore chosen in this study as the exemplary tracer.

3. Model

[11] We consider a horizontally uniform slab of sea ice of thickness h_i covered by a uniform snow cover of depth h_s . At each depth z within the ice, the thermodynamic state of the medium is characterized by a temperature $T(z)$ and a salinity $S(z)$. The size of brine inclusions is characterized by brine volume fraction $e(z)$ (hereafter referred to as brine volume). DSi is assumed to be dissolved within brine and is characterized by a concentration $C(z)$.

3.1. Ice Physics

[12] Ice in the model forms by congelation at the ice base and melts at the upper and lower interfaces depending on interfacial heat budgets. Congelation growth and melt rates are computed using the balance between external heat fluxes, from the atmosphere or the ocean, and internal conductive heat fluxes. The conductive heat fluxes in sea ice are determined from the temperature profile. The temperature profile is the solution of the heat diffusion equation. For a complete description, see the paper by Vancoppenolle *et al.* [2007] and references therein.

[13] Two improvements were made compared to this model version. First, ice now may form in the model from the transformation of snow into ice (snow ice formation). If snow is deep enough to depress the snow-ice interface below the sea level, it is assumed that flooding seawater infiltrates and instantaneously refreezes into the snow (see *Vancoppenolle et al.* [2009a] for details), which forms snow ice. The second improvement to the work of *Vancoppenolle et al.* [2007] is a reformulation of gravity drainage in a more physical way. These two improvements are described below, in addition to a brief summary of the main model characteristics.

3.1.1. Brine Network Domain

[14] The model constitutive equation, which describes the phase equilibrium between ice and brine, is based on two assumptions. First, the freezing temperature T_f (in degree Celsius) of a saline solution is a linear function of its salinity S_{sol} [*Assur*, 1958]:

$$T_f = -\mu S_{\text{sol}}, \quad (1)$$

where $\mu = 0.054^\circ\text{C} \text{‰}^{-1}$. The second assumption is that all the salt is dissolved in the liquid brine inclusions that are at their freezing point in local equilibrium with the surrounding ice. Thus, brine pockets adapt their salinity σ by changing size to the local ice temperature T :

$$T = -\mu\sigma. \quad (2)$$

Because σ and S are related to each other by

$$S = \sigma e, \quad (3)$$

brine volume is only a function of S and T [*Schwerdtfeger*, 1963]:

$$e = -\mu \frac{S}{T}. \quad (4)$$

Close to the sea ice melting point, the brine volume increases drastically. For brine volumes above a threshold of $e_T = 5\%$, the network of brine inclusions connects and sea ice becomes permeable to fluid transport [*Golden et al.*, 1998]. Brine motion is only allowed above that threshold.

3.1.2. Brine Drainage

[15] A general theoretical framework for brine physics is provided by the ‘‘mushy-layer’’ theory [*Worster*, 1992]. Mushy-layers are two-phase, two-component reactive porous media, of which sea ice is an example. The equations presented here constitute a simplification of the exhaustive mushy-layer theory. Assuming that brine motion is purely vertical, the equation governing salt conservation in sea ice is:

$$\frac{\partial}{\partial t} [e\sigma] = -ev_z \frac{\partial \sigma}{\partial z} + \frac{\partial}{\partial z} \left[eD_\sigma \frac{\partial \sigma}{\partial z} \right]. \quad (5)$$

Here, v_z is the vertical velocity of the fluid within the brine network and D_σ is the salt diffusivity in water. At the ice base, we impose σ to be equal to the seawater salinity S_w . At

the ice surface, we impose a boundary condition on the brine flux which depends on the brine drainage mechanism. Assumptions on the brine flow associated with gravity drainage and flushing provide formulations for advective and diffusive terms, respectively. As brine expulsion has been found negligible by *Vancoppenolle et al.* [2006] and *Notz and Worster* [2009], it is ignored in the present model version. In addition, heat transfer associated with brine motion, which might be important but is difficult to quantify at this stage, is neglected.

[16] Flushing is treated as given by *Vancoppenolle et al.* [2007]. If $e \geq e_T$, a volume flux $Q = ev_z$ of interstitial brine moving with velocity v_z and given by

$$Q = \phi \frac{\rho_x}{\rho_w} \frac{dh_x}{dt} \Big|_{\text{su}} I_s \quad (6)$$

can percolate through the brine network. Here, I_s equals 1 if the minimum brine volume $[e_{\text{min}}(z)] \geq e_T$; otherwise, $I_s = 0$. The subscript x refers to either snow or ice, ρ_x is the density of ice/snow, ρ_w is the seawater density, $dh_x/dt|_{\text{su}}$ is the surface melt rate, and $\phi = 0.3$ is the fraction of meltwater allowed to percolate through the brine network. The rest of the meltwater production is assumed to reach the ocean surface through cracks and leads, as suggested by fluorescent tracer experiments in summer Arctic ice [*Eicken et al.*, 2002]. Finally, the percolation term reads:

$$ev_z \frac{\partial \sigma}{\partial z} = Q \frac{\partial \sigma}{\partial z}, \quad (7)$$

i.e., the percolating volume flux Q translates the brine salinity structure downward. At the upper surface, we assume that there is a flux of meltwater Q with zero salinity entering through the uppermost ice layer.

[17] Gravity drainage in our new formulation corresponds to the overturning of brine due to supercritical Rayleigh number in highly porous regions of the ice medium (e.g., skeletal layer and brine channels). Field experiments on the desalination of young sea ice [*Notz and Worster*, 2008] have indicated that convective overturning occurs systematically when the porous medium Rayleigh number

$$Ra = \frac{g(h_i - z)\rho_w\beta_w(\sigma(z) - S_w)\Pi(e_{\text{min}})}{\kappa_i\eta} \quad (8)$$

reaches a critical value of around 10. In the above equation, g is the acceleration due to gravity. $\rho_w\beta_w(\sigma(z) - S_w)$ is the difference between the brine density at level z and that of seawater at the ice-ocean interface. $\Pi(e_{\text{min}})$ is the effective ice permeability (in square meter) computed as a function of the minimum brine volume e_{min} between the level z and the ice-ocean interface. κ_i is the sea ice thermal diffusivity and η is the dynamic viscosity of brine. Convection starts if the driving buoyancy (numerator) is large enough to overcome dissipation (denominator). In the model, it is represented as a mixing process similar to molecular diffusion but characterized by a much larger (turbulent) diffusivity D_σ^{tur} ,

which we estimate to be three orders of magnitude larger than molecular diffusivity, as frequently done to simulate convection in ocean models. Hence, one possible formulation for the diffusive term in equation (5) which appears adequate for the present application is to express the salt diffusivity in brine as a function of Ra :

$$D_{\sigma}(Ra) = I_w[\chi(Ra)D_{\sigma}^{\text{br}} + (1 - \chi(Ra))D_{\sigma}^{\text{mol}}], \quad (9)$$

where D_{σ}^{mol} is the molecular diffusivity of salt in seawater. $I_w = I_w(z)$ is a switch which equals 1 (and 0 otherwise) if $e(z) > e_T$. χ is a partitioning coefficient that favors molecular or turbulent diffusion depending on the Rayleigh number value:

$$\chi(Ra) = \frac{\tanh[A_{\chi}(Ra - Ra_c)] + 1}{2}, \quad (10)$$

with $A_{\chi} = 1$ and $Ra_c = 5$ being the critical Rayleigh number. This formulation ensures that convective motion occurs when $Ra = 10$. Expressed in this form, $\chi(Ra)$ is close to 1 for supercritical values and about 0 for low values of Ra .

[18] The sea ice thermal diffusivity is $\kappa_i(S, T) = \rho_i c_i(S, T) / k_i(S, T)$, where ρ_i , the sea ice density, is assumed constant. The expression for the sea ice specific heat c_i follows *Maykut and Untersteiner* [1971] (and references therein), while the sea ice thermal conductivity k_i is computed using the formula of *Pringle et al.* [2007]. For permeability, following *Notz and Worster* [2008], we use $\Pi = 10^{-17}[10^3 e]^{3.1}$, an empirical expression regressed by *Freitag* [1999] from young sea ice data, which is also reportedly valid for older ice [*Eicken et al.*, 2002]. This regression is very similar to the one of *Golden et al.* [2007], who propose an exponent of 3. At the upper surface, we apply a no-flux boundary condition.

[19] We compare model results obtained using the Ra -based parameterization of gravity drainage with the ones obtained using the classical parameterization of *Cox and Weeks* [1988] which was used in previous model version. On the basis of laboratory measurements, *Cox and Weeks* found that the desalination rate in growing sea ice, which they attributed to gravity drainage, depends on the applied temperature gradient as well as on brine volume:

$$\left. \frac{\partial S}{\partial t} \right|_{gd} = \delta(1 - \eta e) \frac{\partial T}{\partial z}. \quad (11)$$

The formula holds if (1) the temperature gradient is pointing upward and (2) $e > 5\%$, gravity drainage being zero otherwise. δ is an empirical parameter that governs the intensity of the desalination rate and $\eta = 20$. *Cox and Weeks* [1988] suggested the value $\delta_{\text{lab}} = 1.68 \times 10^{-7} \text{‰ m } (\text{°C s})^{-1}$ from observations, while *Vancoppenolle et al.* [2007] proposed to use $\delta_{\text{mod}} = 5.88 \times 10^{-8} \text{‰ m } (\text{°C s})^{-1}$, to improve the simulated salinity profile. In *Cox and Weeks* [1988] formulation of gravity drainage, no brine flow is computed; hence, the computation of the transport of a dissolved tracer is difficult. The new parameterization of gravity drainage, based on an advection-diffusion equation for brine salinity over the nonuniform brine network, accommodates dissolved tracers easily.

3.1.3. Ice-Ocean Salt Flux

[20] Some salt is trapped into ice when it forms and is then rejected by different means, which is formalized using an ice-ocean salt flux F^s [kg NaCl m s^{-1}]:

$$F^s = F_{b,+}^s + F_{si}^s + F_{bd}^s + F_{b,-}^s + F_{su}^s. \quad (12)$$

The terms on the right-hand side correspond to the contributions of basal congelation, formation of snow ice, brine drainage, basal melt, and surface melt, respectively, and are considered as positive from the ice to the ocean.

[21] In the case of growing ice without surface seawater flooding, only the contributions of basal growth and brine drainage are present, which in the model are computed using:

$$F_{b,+}^s = -\frac{\rho_i}{1000}(1 - \nu_b)S_w \frac{\partial h_{i,b+}}{\partial t}, \quad (13)$$

$$F_{bd}^s = -\frac{\rho_i}{1000} \left[e D_{\sigma} \frac{\partial \sigma}{\partial z} \right]^{z=h}. \quad (14)$$

3.1.4. Sources of Salt in Sea Ice

[22] We consider two sources of salt intrusion within sea ice. First, salt remains in sea ice during basal ice growth. Following *Cox and Weeks* [1988], the salinity of new ice is given by

$$S_b = \nu_b S_w, \quad (15)$$

where ν_b is a fractionation coefficient that was historically prescribed as a function of the ice growth rate [*Cox and Weeks*, 1988]. Observations by *Notz and Worster* [2009] and sensitivity experiments described in section 3 suggest to use $\nu_b = 1$ instead.

[23] Second, there is salt input at the ice surface associated with flooding of snow by seawater and subsequent snow ice formation. In the model, the salinity of new snow ice is assumed to be

$$S_{si} = \nu_{si} \left[\frac{\rho_i - \rho_s}{\rho_i} \right] S_w, \quad (16)$$

where ρ_s is the snow density and ν_{si} is a tuning coefficient that specifies how much salt is initially trapped into the snow ice. ν_{si} is equal to 1 by default in the model.

3.2. Ice Biophysics

[24] In order to highlight biophysical interactions, the biophysical component consists of one nutrient (DSi) dissolved within brine, transported by fluid motion, and removed through primary production (prescribed). Sophisticated biological processes, such as nutrient limitation of primary production, remineralization by bacteria, or dissolution of diatom frustules, are neglected in order to isolate the first-order biophysical coupling.

3.2.1. Nutrient Mass Conservation Equation

[25] The dissolvable macronutrients (here DSi) are treated in the model as passive tracers dissolved in brine inclusions

following liquid motion. Hence, the concentration of nutrients within the ice are also solutions of advection-diffusion equations. DSi, as any passive tracer dissolved in brine, is characterized in the model by bulk (i.e., ice plus brine) concentration $C(z)$. By analogy to the ice salinity (equation (3)), bulk and brine (ζ) DSi concentrations are related through

$$C = \zeta e. \quad (17)$$

Units used here are molar concentrations (mmol m^{-3}). The nutrient mass conservation equation for DSi reads:

$$\frac{\partial}{\partial t}[e\zeta] = S_\beta - Q \frac{\partial \zeta}{\partial z} + \frac{\partial}{\partial z} \left[e D_\sigma \frac{\partial \zeta}{\partial z} \right], \quad (18)$$

where S_β refers to the biochemical sources and sinks, and the two last terms refer to nutrient transport and mixing due to flushing and gravity drainage, respectively.

3.2.2. Nutrient Flux at the Ice Base

[26] At the ice base, we impose ζ to be equal to the concentration of DSi in seawater C_w . The DSi flux associated with brine drainage F_{bd}^{DSi} [$\text{mmol m}^{-2} \text{s}^{-1}$] is given by

$$F_{bd}^{\text{DSi}} = \left[-e D_\sigma \frac{\partial \zeta^{\text{DSi}}}{\partial z} \right]_{z=h} \quad (19)$$

and is assumed positive for a transfer from the ice to the ocean.

3.2.3. Sources of Nutrient

[27] As for salt, two sources of DSi intrusion within sea ice are considered. First, DSi remains in sea ice during basal ice growth and the bulk tracer concentration in basal new ice is given by

$$C_b = \nu_b C_w. \quad (20)$$

Second, there is DSi input associated with snow ice formation, with a concentration given by

$$C_{si} = \nu_{si} \left[\frac{\rho_i - \rho_s}{\rho_i} \right] C_w, \quad (21)$$

assuming for simplicity a zero concentration in the snow.

3.2.4. Uptake by Primary Production

[28] Here, for simplicity, biochemical sources and sinks are reduced to algal uptake of DSi. Assuming that all the primary production is due to diatoms, the uptake of silica is given by

$$S_\beta = -\text{PP} \frac{\text{Si}}{C}, \quad (22)$$

where Si/C is the silicate-to-carbon ratio. Following primary production (PP) estimates from winter Weddell Sea pack ice [Kottmeier and Sullivan, 1987], we choose a constant value for PP of $35 \text{ mg C}/(\text{m}^2 \text{ d})$, which corresponds to $3.3 \times 10^{-5} \text{ mmol C m}^{-3} \text{ s}^{-1}$. PP is assumed nonzero only if the

incoming shortwave radiation $F^{\text{SW}} > 0$. In order to mimic the effect of a bottom community, PP is uniformly distributed only over the three lowermost ice layers. According to the review by Sarthou *et al.* [2005], most diatom species have a silicate-to-carbon molar ratio Si/C between 0.05 and 0.19. Hence, we use a mean value Si/C = 0.12. Obviously, the formulation of primary production could be more complex, e.g., depending on light or on the availability of nutrients, but was kept simple for the present study.

3.2.5. Nutrient Budget in the Model

[29] In order to assess the impact of primary production on nutrient uptake, the net DSi budget in the sea ice column was computed over the ice growth period. The sea ice DSi content in the liquid phase at a given time t is defined as: $M^{\text{DSi}}(t) = \int_0^h C(z, t) dz$ [mmol m^{-2}]. Integrating equation (18) over the ice column between two instants t_0 and t_1 , the sea ice nutrient budget, in the absence of melting, reads:

$$[M^{\text{DSi}}]_{t_0}^{t_1} = M^{\text{DSi}}(t_1) - M^{\text{DSi}}(t_0) = B + \text{SI} + \text{BD} + \beta. \quad (23)$$

B , SI, BD, and β are the sources/sinks of DSi content [mmol m^{-2}] associated with basal congelation, snow ice formation, brine drainage, and algal uptake, respectively, integrated over the ice column between t_0 and t_1 .

3.3. Numerics

[30] The salt and tracer transport equations (5) and (18) are solved in the framework of a thermodynamic sea ice model (see Figure 1 for a sketch of model grid). The thermodynamic component used here is from Vancoppenolle *et al.* [2007], which is based on the Bitz and Lipscomb [1999] 1D energy-conserving model. Prognostic variables are h_i , h_s , $T(z)$, $S(z)$, and $C(z)$. Temperature variations are computed by numerically solving the heat diffusion equation in one layer of snow (temperature T_s) and N layers of sea ice, characterized by their temperature T_k and salinity S_k ($k = 1, \dots, N$).

[31] Layer midpoints are referenced by a vertical coordinate z_k ($k = 1, \dots, N$) and their thicknesses are given by Δz_k (see Figure 1). In order to represent the effect of brine inclusions on heat transfer and storage, the sea ice thermal properties depend on S and T . The growth (melt) rates at the interfaces are computed by dividing the heat loss (gain) F by $q(S, T)$, the energy of melting. Shortwave radiative transfer is accounted for as follows: surface albedo in the model is 0.80 for dry snow, 0.65 for melting snow, and 0.50 for bare ice. Most of the incoming solar radiation contributes to the surface energy budget, but a fraction i_0 , equal to 0.15 if snow is present and to 0.30 otherwise, penetrates in the snow-ice system. Radiation decay in sea ice follows Beer's law. The extinction coefficients for snow and ice are 15 and 0.8 m^{-1} , respectively, following field observations [Grenfell and Maykut, 1977; Grenfell *et al.*, 2006; Light *et al.*, 2008].

[32] The steps of the computation of T_k , S_k , and C_k ($k = 1, \dots, N$) within the computer code are the following (see Figure 2): (1) radiative transfer; (2) diffusion of heat; (3) transport of salt and tracer; (4) sources and sinks of ice mass, salt, and tracer; (5) recomputation of the grid due to ice growth and melt; and (6) conservative remapping of ice thermal, salt, and tracer contents on the new grid.

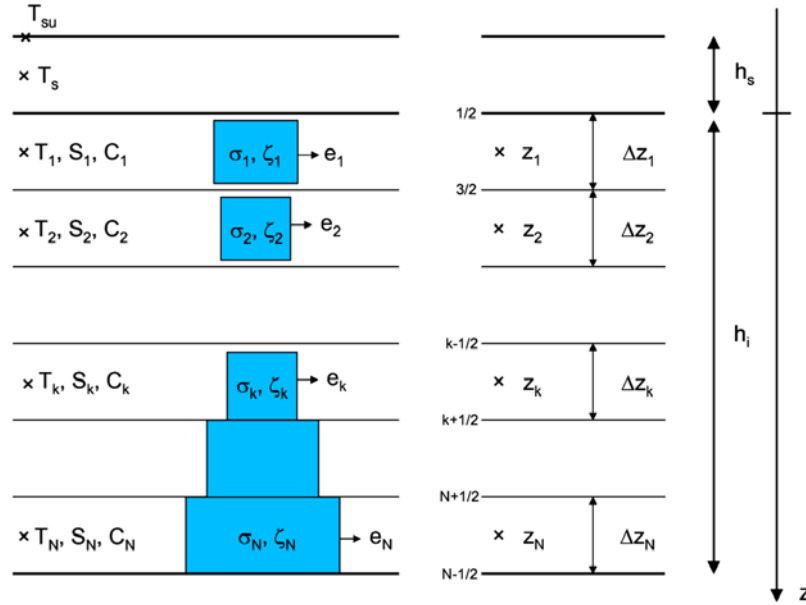


Figure 1. Vertical configuration of variables on the model grid; h_i is the ice thickness and h_s is the snow depth. T_{su} , T_s , and T_k ($k = 1, \dots, N$) refer to the surface, snow, and ice temperatures, respectively. The term N represents the number of ice layers. The terms S_k and C_k (σ_k and ζ_k) are the bulk (brine) ice salinities and tracer concentrations, while e_k refers to the brine volumes. The z_k are the layer vertical coordinates and Δz_k their thicknesses.

[33] The salt and tracer transport equations (5) and (18) are solved using a finite difference, implicit, numerical scheme, which conserves salt and tracer mass within computer precision. At each time step, we solve [5] for σ , keeping e fixed and then compute S by restoring thermal equilibrium within the ice using $S = \sigma e$. Sources of new ice salinity and tracer are computed using equations (15), (16), (20), and (21). Each of the steps ensures the conservation of the volume of equivalent meltwater, salt, tracer, and heat

contents, summed over the whole snow-sea ice column. The volume of equivalent meltwater [kg m^{-2}] is given by

$$V^w = \rho_s h_s + \sum_{k=1}^N \rho_i \Delta z_k; \quad (24)$$

the total salt content [$\% \text{ m}^{-2}$] is

$$M^s = \sum_{k=1}^N S_k \Delta z_k; \quad (25)$$

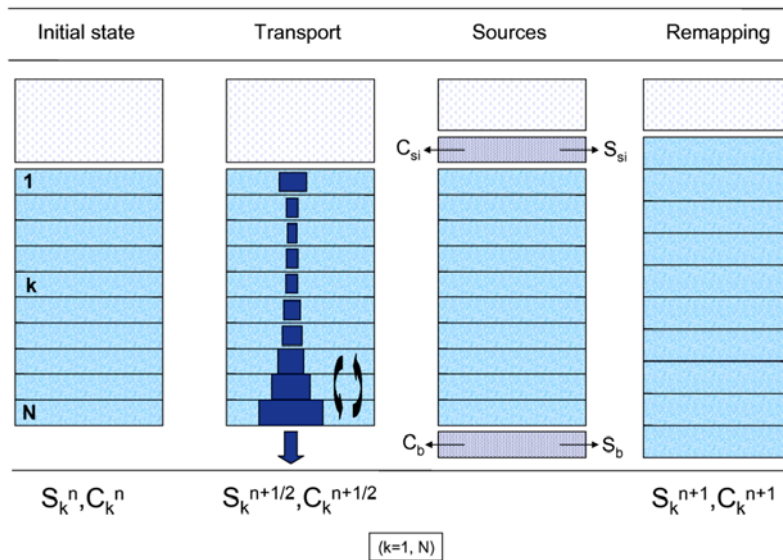


Figure 2. Successive steps in the computation of ice salinity and bulk tracer content: transport, sources, and remapping.

Table 1. List of Model Parameters and Constants for the Control Run CTL

Variable	Definition	Value	Units
ν_b	Basal salt fractionation coefficient	1	-
ν_{si}	Snow ice salt fractionation coefficient	1	-
e_T	Brine volume permeability threshold	0.05	-
g	Acceleration due to gravity	9.81	m s^{-2}
A_Y	Convection decision coefficient	1	-
D_{σ}^{tur}	Turbulent diffusivity of salt in water	10^{-6}	$\text{m}^2 \text{s}^{-1}$
D_{σ}^{mol}	Molecular diffusivity of salt in water	6.8×10^{-10}	$\text{m}^2 \text{s}^{-1}$
N	Number of vertical ice layers	10	-
Ra_c	Critical Rayleigh number for convection	5	-
S_w	Seawater salinity	34	‰
C_w	Concentration of DSi in seawater	40	mmol m^{-3}
η	Dynamic viscosity of brine	1.79×10^{-3}	$\text{kg m}^{-1} \text{s}^{-1}$
μ	Freezing point coefficient	0.054	$^{\circ}\text{C } \text{‰}^{-1}$
ϕ	Fraction of percolating surface meltwater	0.3	-
ρ_w	Seawater density	1025	kg m^{-3}
ρ_i	Sea ice density	917	kg m^{-3}
ρ_s	Snow density	330	kg m^{-3}
F^w	Oceanic heat flux	5	W m^{-2}
PP	Primary production rate	3.3×10^5	$\text{mmol C m}^{-3} \text{s}^{-1}$
Si/C	Silicon-to-carbon molar ratio in diatoms	0.12	-

the total tracer content [kg m^{-2}] is defined by

$$M^c = \sum_{k=1}^N C_k \Delta z_k; \quad (26)$$

the total heat content is defined by [J m^{-2}]

$$Q = q_s(T_s)h_s + \sum_{k=1}^N q_i(S_k, T_k)\Delta z_k, \quad (27)$$

where $q_s(T)$ and $q_i(S, T)$ are the snow and sea ice energies of melting, respectively. The energy of melting is defined as the heat required to warm a unit volume of snow or sea ice from a temperature T to a given energy reference level (see, e.g., *Bitz and Lipscomb* [1999] and *Schmidt et al.* [2004] for a detailed discussion and *Hunke and Lipscomb* [2004] for a definition). Because we assume that the densities of ice, brine, and seawater are constants, the volume of meltwater rather than mass is conserved. Though not physically realistic, this only introduces minor errors and is consistent with Boussinesq ocean models that conserve seawater volume and not mass.

4. Experimental Setup

[34] The experimental setup was designed to run a series of simulations of the seasonal growth and decay of first-year Antarctic sea ice, sequentially reproducing the three major ice types observed within the Antarctic sea ice pack: *unflooded winter ice*, *flooded ice*, and *summer ice*.

4.1. Forcing

[35] We use forcing fields from the mean geographical coordinates of the Ice Station POLarstern (ISPOL) drift station (see section 4.4 for a description) in 2004. Daily NCEP/NCAR 2 m air temperatures and 10 m winds for year 2004 [*Kalnay et al.*, 1996] as well as monthly climatological cloud fraction and humidity are combined using standard formulas to compute radiative and turbulent heat fluxes from the atmosphere [see *Goosse*, 1997, for details]. An oceanic heat flux of 5 W m^{-2} , following observed mean value in Weddell Sea in winter [*Lytte and Ackley*, 1996] is imposed. Following ECMWF reanalyzes [see *Maksym and Markus*, 2008, Figure 2], the snowfall rate is set to 1.8 mm d^{-1} if the air temperature is under 273.15 K and 0 otherwise. According to the World Ocean Circulation Experiment (WOCE) atlas [*Conkright et al.*, 2001], the concentration of DSi in seawater is typically $C_w = 40 \text{ mmol m}^{-3}$ in the Weddell sea. A list of relevant model constants and parameters is provided in Table 1.

4.2. Initialization

[36] The model simulation starts on 13 February, a typical date for the restart of new ice growth, and ends on 31 December. The model's initial conditions are: $h_i = 10 \text{ cm}$, $h_s = 2 \text{ cm}$, and $S = 13.6\text{‰}$ at each depth. From values measured in young Antarctic sea ice [*Dieckmann et al.*, 1991], an initial value of $C = 15 \text{ mmol m}^{-3}$ at each depth is chosen. The initial value of the surface temperature is $T^{\text{su}} = 265 \text{ K}$. For the rest of the values, we assume a linear profile within ice and snow, the basal interface being at the seawater freezing point $T_w = -\mu S_w$.

[37] The number of vertical layers ($N = 10$) is chosen in order to produce smooth profiles that are best comparable to the observational data we used, which have comparable resolution. However, for a realistic simulation of the main features of vertical salinity, tracer concentration, and temperature profiles, sensitivity experiments show that $N = 5$ layers is enough (run 05 in Table 2). Finally, using $N = 3$ layers, induces changes in ice thickness only within 1 cm compared to $N = 10$ (run 06).

4.3. Sensitivity Experiments

[38] Several sensitivity experiments (listed in Table 2) were performed and are referred to throughout the text. A first series of runs involves changes to the snowfall rate and algal uptake (runs 02–04). The runs with higher snowfall (runs 02, 04, and 10) correspond to observations in Bellingshausen and Amundsen Seas. The sensitivity to the number of layers (runs 05 and 06) is tested in a second ensemble of simulations. A third series of experiments is dedicated to compare the control run (CTL) to the classical parameterizations of *Cox and Weeks* [1988] for (1) salt fractionation at the ice base (run 07) and (2) desalination rate due to gravity drainage as a function of the temperature gradient (runs 08–10). The fourth ensemble of runs aims at testing the impact of parameters that control vertical mixing, namely Ra_c and D_{σ}^{tur} (runs 11–15). Finally, the nature of the mixing process (diffusive or turbulent) is tested (runs 16–19).

Table 2. Description of the Model Sensitivity Runs^a

Run Number	Name	N	D_{σ}^{tur}	Ra_c	Grav. dr.	ν_b	SF	PP
<i>Control Run</i>								
01	CTL	10	10^{-6}	5	$D_{\sigma} = D_{\sigma}(Ra)$	1	1.8	off
<i>Sensitivity to Snowfall Rate and Algal Uptake</i>								
02	2SNOW	10	10^{-6}	5	$D_{\sigma} = D_{\sigma}(Ra)$	1	3.6	off
03	CTL_BIO	10	10^{-6}	5	$D_{\sigma} = D_{\sigma}(Ra)$	1	1.8	on
04	2SNOW_BIO	10	10^{-6}	5	$D_{\sigma} = D_{\sigma}(Ra)$	1	3.6	on
<i>Sensitivity to Vertical Resolution</i>								
05	5LAY	5	10^{-6}	5	$D_{\sigma} = D_{\sigma}(Ra)$	1	1.8	off
06	3LAY	3	10^{-6}	5	$D_{\sigma} = D_{\sigma}(Ra)$	1	1.8	off
<i>Sensitivity to Bottom Boundary Condition; Gravity Drainage as in Work by Cox and Weeks [1988]</i>								
07	NCW	10	10^{-6}	5	$D_{\sigma} = D_{\sigma}(Ra)$	CW88	1.8	off
08	CW_LAB	10	n.a.	n.a.	CW88, δ_{lab}	CW88	1.8	off
09	CW_MOD	10	n.a.	n.a.	CW88, δ_{mod}	CW88	1.8	off
10	2SNOWCW	10	n.a.	n.a.	CW88, δ_{mod}	CW88	3.6	off
<i>Sensitivity to Vertical Mixing Parameters</i>								
11	RAC10DT6	10	10^{-6}	10	$D_{\sigma} = D_{\sigma}(Ra)$	1	1.8	off
12	RAC05DT7	10	10^{-7}	5	$D_{\sigma} = D_{\sigma}(Ra)$	1	1.8	off
13	RAC10DT7	10	10^{-7}	10	$D_{\sigma} = D_{\sigma}(Ra)$	1	1.8	off
14	RAC05DT8	10	10^{-8}	5	$D_{\sigma} = D_{\sigma}(Ra)$	1	1.8	off
15	RAC10DT8	10	10^{-8}	10	$D_{\sigma} = D_{\sigma}(Ra)$	1	1.8	off
<i>Sensitivity to Mixing Process (Diffusive or Turbulent)</i>								
16	DMOL_N1	10	n.a.	5	$D_{\sigma} = D_{\sigma}^{\text{mol}}$	1	1.8	off
17	DTUR_N1	10	10^{-6}	5	$D_{\sigma} = D_{\sigma}^{\text{tur}}$	1	1.8	off
18	DMOL_NCW	10	n.a.	5	$D_{\sigma} = D_{\sigma}^{\text{mol}}$	CW88	1.8	off
19	DTUR_NCW	10	10^{-6}	5	$D_{\sigma} = D_{\sigma}^{\text{tur}}$	CW88	1.8	off

^aN is the number of ice layers, Ra_c is the critical Rayleigh number, ν_b the basal entrainment coefficient, SF the snowfall rate (mm d^{-1}). PP refers to the algal uptake associated with primary production. Grav. dr. refers to the representation of gravity drainage used, either using a salt diffusivity or based on Cox and Weeks [1988] (CW88). D_{σ} is the salt diffusivity in brine (m^2/s) and D_{σ}^{tur} and D_{σ}^{mol} are the turbulent and molecular salt diffusivities, respectively. D_{σ} can either be prescribed (to D_{σ}^{mol} or D_{σ}^{tur}) or computed as a function of the Rayleigh (Ra) number (see equation (9)).

4.4. Observations Used for Model Validation

[39] For each ice type, in situ observations of sea ice salinity and DSi concentration from two Antarctic sea ice drift stations were selected for comparison with the model results.

[40] The ISPOL drift station took place in the Western Weddell Sea from 27 November 2004 to 3 January 2005 within a 67–68.5°S latitude range and a 54–56°W longitude range. Vertical profiles of physical and biogeochemical properties were measured from ice core sections. Sampling was performed every five days on seven occasions, from nearby locations on an homogeneous sampling site [see Tison *et al.*, 2008]. A major concern was to select an unflooded (positive freeboard), level first-year sea ice area. Ice thickness was 80–90 cm and snow depth was 10–25 cm. Ice texture was mostly columnar. On the first visit (29 November), the extracted sea ice cores were still relatively cold. Hence, ISPOL visit 1 is considered here as a reference for *cold, unflooded ice*. The latter assumption seems valid as the ISPOL visit 1 profile is very similar to the typical salinity profiles from cold, unflooded sea ice [e.g., Eicken, 1992; Vancoppenolle *et al.*, 2007]; see symbols on Figure 4a. In the course of December, ice warming and melting progressed at ISPOL. Intrusions of snow fresh meltwater flowing laterally inside the ice were detected on several occasions, notably on the third and sixth visit (25 Dec). The latter is considered in this study as a reference for *summer ice*. At ISPOL, the highest Chla values (up to $30 \mu\text{g l}^{-1}$) were consistently found in the lowest 10 cm of the ice cover and remained fairly constant (within $1\text{--}2 \mu\text{g l}^{-1}$) elsewhere. The bottom layers were overwhelmingly occupied by pennate diatoms (98–100% of the biomass) [Dumont, 2009].

[41] The Ice Station Belgica (ISB) was part of the SIMBA-IPY (Sea Ice Mass Balance in the Antarctic-International Polar Year) cruise that took place in the Bellingshausen Sea over September and October 2007 (P.I. S. Ackley; co-P.I. J.-L. Tison). The ISB was established on a floe located within (69°S–71°S and 92°E–95°E). The same methods as at ISPOL were applied to perform biophysical measurements from ice core sections [Tison *et al.*, 2007]. Two sampling sites, established on the ISB floe and named “Brussels” and “Liège” were visited once every 5 days. In the present study, we use measurements at the Liège site, which was characterized by 90–110 cm thick granular ice and 30–40 cm deep snow, i.e., much deeper than at ISPOL. Deep snow triggered frequent surface flooding. Hence, we consider the latter as a reference for *flooded ice*. Profiles averaged over the five visits at the Liège site are used here. At ISB (Liège), the Chla ranged from 1.1 to $25.7 \mu\text{g l}^{-1}$, with maximum value in the vicinity of the surface. The surface community was composed of dinoflagellates and Phaeocystis sp. cells, while the bottom community mostly consisted of diatoms [Dumont, 2009].

[42] Finally, in order to evaluate the simulated ice-ocean salt flux, we use laboratory observations performed during the growth of artificial sea ice [Wakatsuchi and Ono, 1983] (hereafter WO83). The reader should remember that the ice growth rates of WO83 are rather high, typical of new ice formation, which may not be consistent with the simulations presented here.

5. Results

[43] An overview of the simulated evolution of the ice pack salinity and thickness is given in Figure 3. The ice growth starts moderately in February and then accelerates

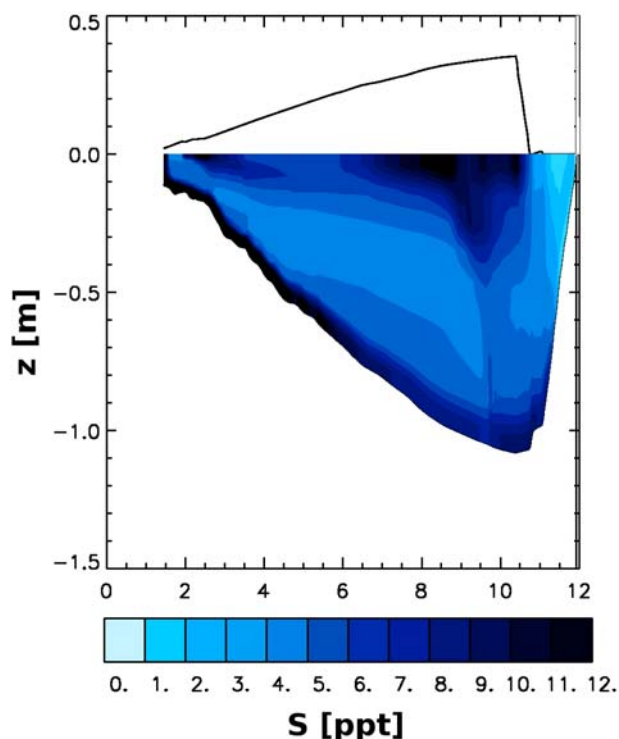


Figure 3. Time series of S contoured in the snow-ice domain for run CTL. Horizontal axes refer to months. Vertical axes represent depths as referred to the snow-ice interface.

until the maximal ice thickness is reached (1.1 m) in mid-October, which is close to the first-year pack ice thickness in the Weddell Sea observed at the beginning of the melt season [e.g., Haas *et al.*, 2008; Tison *et al.*, 2008]. Then, on 24 November, ice begins to melt rapidly. Snow depth evolution is the result of the balance between snowfall (source), snow ice formation and snowmelt (sinks). Snow ice formation starts in early June and intensifies in September. Snowmelt begins on 14 November and ends on 24 November, which is at least one month earlier than

reported from observations [Haas *et al.*, 2008]. The simple snow scheme we use is well known to melt snow too rapidly (see sensitivity experiments in Vancoppenolle *et al.* [2007]). Partly for this reason, ice also melts too early and rapidly. It is likely that a better snow model would reduce snowmelt and improve the results [see, e.g., Nicolaus *et al.*, 2006]. Other sources of error in the rate of summer melt are the incoming long-wave radiation and oceanic heat flux. As the purpose of the present study is rather an investigation of nutrient transport physics than an exact validation of the mass balance, we will not investigate further the sources of error in ice thickness and snow depth here. For a more in-depth analysis, see Vancoppenolle *et al.* [2007]. There is ongoing work to improve the snow model (O. Lecomte, personal communication) and to assess uncertainties in the forcings.

[44] The three analyzed ice types can be clearly distinguished from the temporal evolution of ice thickness and snow depth, depending on the rates of basal growth, snow ice formation, and surface melt. The three types are characterized by vertical profiles of S and C that differ profoundly. In the CTL simulation (see Table 2), unflooded cold ice typically develops between April and June, flooded ice is simulated from September to mid-November, and summer ice from mid-November to the end of December. We focus on those three regimes rather than the exact limit dates of each period.

5.1. Comparison of Simulated Profiles With Observations

5.1.1. Simulated Salinity Profiles

[45] The simulated S profile is compared to observations for the three reference thermodynamic regimes in order to assess the model ability to simulate brine drainage and its effect on the salinity profile (Figure 4). In the early months of the simulation (April–June), unflooded sea ice is only affected by basal congelation. Salt is trapped at ice base and released by gravity drainage in the lowermost, porous ice layers. Consequently, the S profile exhibits a typical C-shape reported in many instances [e.g., Nakawo and Sinha, 1981; Eicken, 1992]. The simulated S profile is close to observations performed in unflooded cold ice (ISPOL visit 1),

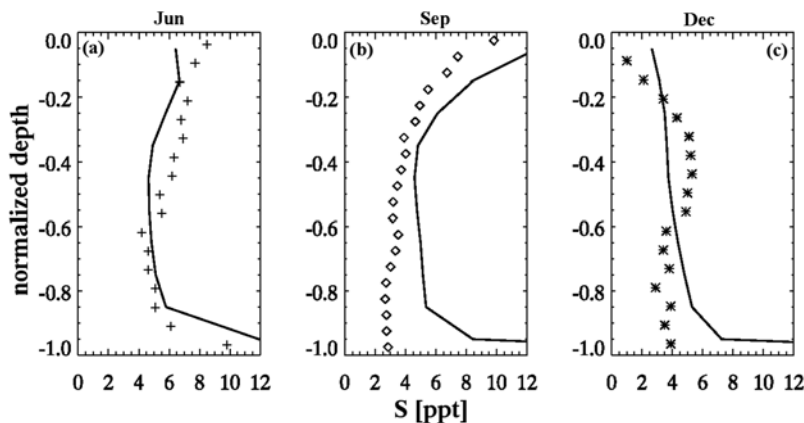


Figure 4. Vertical profiles of S (solid line) as a function of normalized depth (z/h_i) for run CTL: (a) June, (b) September, and (c) December. For comparison, field observations of S are also shown: ISPOL visit 1 (pluses), ISB (Liège site, stations 1–5, diamonds), ISPOL visit 6 (stars). Simulated ice salinity reaches S_w near the ice base. Axis was cut to magnify differences within the ice.

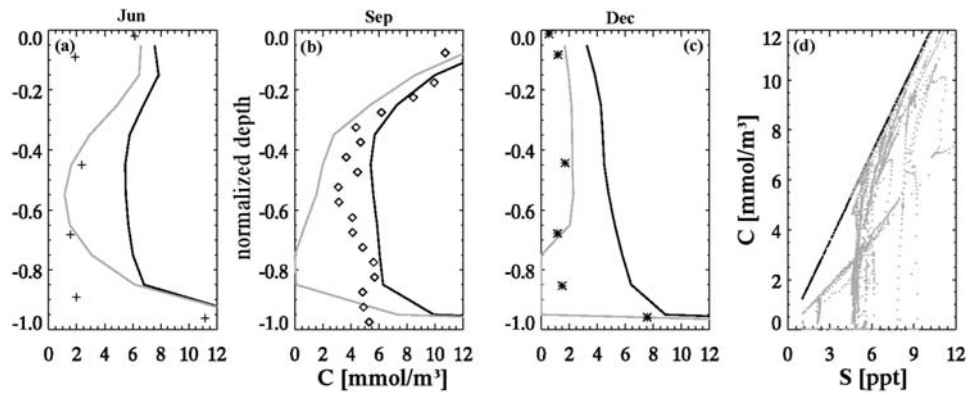


Figure 5. Normalized vertical profiles of the ice concentration of DSi (C): (a) June, (b) September, (c) and December for runs CTL (black) and CTL_BIO (gray). For comparison, field observations of C are also shown: ISPOL visit 1 (pluses), ISB (Liège site, stations 1–5) (diamonds), ISPOL visit 6 (stars). At the ice base, $C = C_w$. Horizontal axis was cut to magnify differences within the ice. (d) Scatterplot of C as a function of S .

with a notable exception near the base, where salinity is overestimated by the model. Nevertheless, salinity measurements performed by the means of nondestructive methods suggest that brine drainage in the lowermost ice layers during ice core extraction may lead to an underestimation of ice salinity by 10‰ [Notz *et al.*, 2005]. Other model-observation differences upper in the ice are difficult to interpret because of large spatial variability due to local variations in ice thickness and snow depth [Eicken *et al.*, 1991].

[46] *Flooded ice* is characterized by higher salinity values near the surface. In September and October, due to the deep snow cover, infiltrating seawater floods the base of the snow and associated snow ice formation occurs in the model. Similar salinity profiles have been found by Eicken [1992] to occur frequently in Antarctic sea ice. For comparison, we show the S profile from sea ice cores extracted at Liège site during the ISB drift station (Figure 4). Near the surface, the model agrees well with observations. Near the ice base, the model and observed profiles substantially differ. This is very likely due to the fact that the ice grows in the model at the ice base, while it was melting most of the time at ISB.

[47] Finally, during the summer period, snow and sea ice melt. The resulting fresh meltwater percolates through the open brine network and replaces the saline brine. This process has been described in detail by Vancoppenolle *et al.* [2007]. Flushing is probably not typical of Antarctic sea ice, as suggested by the large-scale ice core collection analysis and modeling study of Vancoppenolle *et al.* [2009b], although it has been found to occur in some instances. Eicken [1992] reported that this process may occur in the Weddell Sea, being usually restricted to second-year and multiyear ice and dependent on the proximity to the ice edge. S profiles with near-zero values in the vicinity of the surface have been reported recently in summer Weddell Sea pack ice during the ISPOL field campaign [Tison *et al.*, 2008; Haas *et al.*, 2008]. The details of the profile are nevertheless not reproduced, since flushing is a threshold process dependent on the snow cover and hence subject to substantial horizontal variability [e.g., Haas *et al.*, 2008].

5.1.2. Simulated DSi Profiles

[48] Given the uncertainties on mass balance and the very crude representation of primary production in the model, the comparison of DSi profiles to observations is rather qualitative. The DSi observations used here were derived from ice cores from the ISPOL and ISB drift stations. The sites and times of extraction correspond to the ones of the S profiles used in the previous subsection.

[49] The largest simulated concentrations of DSi are found near the ice surface and near its base. As expected, DSi concentrations are generally lower when algal uptake is activated (CTL_BIO) than when it is not (CTL). In abiotic conditions, S and C are driven in the model by the same processes and their evolution equations (3), (20) have the same form. Hence, at each depth within the ice, S and C differ only by a multiplication constant and their values lie on the dilution line extrapolated from their original concentrations in seawater. In run CTL_BIO, algal uptake of nutrients decreases the DSi– S ratio. Hence, the simulated values of C lie below the dilution curve (Figure 5), in agreement with various field observations [e.g., Dieckmann *et al.*, 1991; Tison *et al.*, 2008; Fripiat *et al.*, 2007]. Algal uptake reduces C in particular near the ice base where the bloom is assumed to take place (see Figures 5a–5c). Similar depletion of C near the ice base were found in spring Weddell Sea pack ice [Clarke and Ackley, 1984] as well as in late spring sea ice of the Canadian Archipelago after a bloom [Cota *et al.*, 1987].

[50] The shape of the C profile for *unflooded ice* in CTL_BIO (see Figure 5a) is qualitatively similar to observations. This is particularly true in the lower half of the ice and less the case near the surface, where C is overestimated by the model. Possible causes of discrepancy are uncertainties in primary production and in the concentration of DSi in seawater. In September–October, seawater flooding forces nutrient input near the ice surface that slowly percolates toward the base, resulting in higher DSi concentrations in the vicinity of the surface, as observed in the *flooded ice* of ISB. The factors that may explain the near-surface overestimation of C by the model are: (1) the

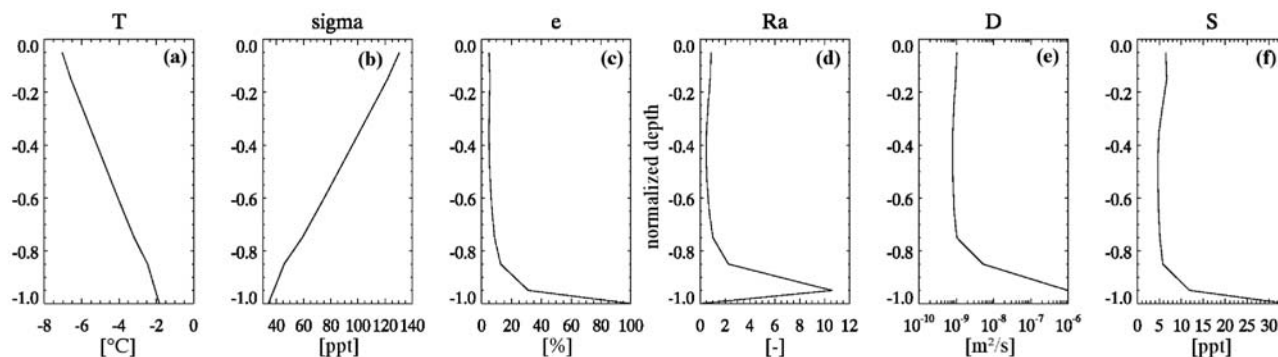


Figure 6. Normalized vertical profiles of (a) temperature, (b) brine salinity, (c) brine volume fraction, (d) Rayleigh number, (e) diffusivity, and (f) ice salinity, averaged over June, for run CTL.

loss of nutrient dissolved in brine during core extraction and (2) the simulation of basal ice growth in September by the model, not observed at ISB. In summer, nutrients are flushed out by the downward percolation of nutrient-free surface meltwater.

5.2. Unflooded Cold Ice Dynamics: Role of Gravity Drainage

[51] We now analyze in more detail the simulated gravity drainage, which shapes the salinity profile of unflooded, cold ice. Gravity drainage is forced by the temperature gradient pointing downward, which induces smaller and more saline brine inclusions at higher levels in the ice (Figure 6). Due to changes in ice porosity and brine salinity, the Rayleigh number peaks at values around 10 in the lowermost 5 cm of the ice. Convection strength, represented in the model by values of D_σ close to D_σ^{tur} , and the associated desalination rate are maximum near the ice base. At higher levels in the ice, the brine column is stable: the nonlinear decrease in permeability due to lower brine volume dominates the linear increase in brine salinity and brings the Rayleigh number back to subcritical levels. In summary, brine overturning is more intense in the lowermost, more saline, and more permeable ice layers, and practically nonexistent elsewhere.

5.2.1. Sensitivity of the Salinity Profile to Model Parameters

[52] Rayleigh-number-dependent convective mixing in the lowermost layers is required to simulate the typical winter sea ice salinity profile. Sensitivity experiments to Ra_c and D_σ^{tur} demonstrate clearly this point. Those two parameters, not well constrained by observations, control the intensity and timing of convective mixing. Lower values of the threshold Ra_c and higher values of D_σ^{tur} induce more frequent and stronger overturning, respectively. Given the uncertainty in Ra_c and D_σ^{tur} , their numerical values were adjusted as part of the model calibration. In Figure 7, the simulated $Ra(z)$ and $S(z)$ for several sensitivity experiments to Ra_c and D_σ^{tur} are shown. The results indicate that D_σ^{tur} has to be at least $10^{-7} \text{ m}^2 \text{ s}^{-1}$ to produce sufficient desalination. A value of $10^{-8} \text{ m}^2 \text{ s}^{-1}$ results in $S = 7\text{--}15\%$ in the interior of the ice, which is much larger than observations. Results also suggest an optimal value of Ra_c around 5 since $Ra_c = 10$ inhibits desalination too rapidly.

5.2.2. Comparison to Other Formulations

[53] We now compare the simulated salinity profile in the control run to various hypotheses on the mechanisms of winter sea ice desalination. In a first series of sensitivity experiments (runs 16–19 in Table 2), the impact of changing the salt diffusivity in brine was tested (Figure 8). In

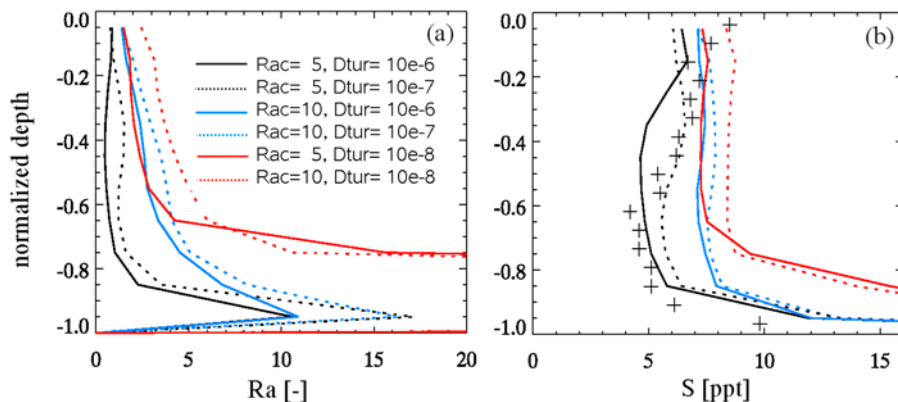


Figure 7. Simulated vertical profiles of (a) Rayleigh number and (b) sea ice salinity, in June, for different Ra_c and D_σ^{tur} values. For reference, field observations of S are also shown: ISPOL visit 1 (pluses).

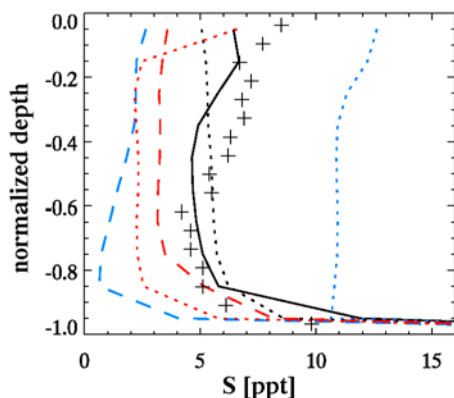


Figure 8. Impact of the model representation of gravity drainage physics on the simulated vertical salinity profile (June). Different simulations are shown: resolving brine transport (run CTL, solid black curve); assuming salt fractionation at the ice base (run NCW, black dotted curve); assuming pure molecular diffusion or turbulent mixing (run DMOL_NCW, blue dotted curve); run DTUR_NCW (blue dashed curve). Runs for which gravity drainage is computed using the parameterization of *Cox and Weeks* [1988] (run CW_MOD, red dotted curve; run CW_LAB, red dashed curve) are also shown. For comparison, field observations of S were added (ISPOL, visit 1, pluses).

DTUR_NCW, $D_\sigma = D_\sigma^{\text{tur}}$ at all depths, i.e., brine mixing is convective only. Desalination in DTUR_NCW is too strong and S is consequently underestimated. In contrast, in DMOL_NCW, $D_\sigma = D_\sigma^{\text{mol}}$ at all depths and the desalination is too weak ($S = 8\text{--}10\text{‰}$ in the inner ice layers). In a second series of sensitivity runs (08 and 09), the empirical parameterization of *Cox and Weeks* [1988], based on laboratory measurements, was used to compute the desalination rate due to gravity drainage. In the latter, gravity drainage is a function of the local temperature gradient and is only active in regions where the brine volume is above 5%. The results indicate that with the original gravity drainage intensity parameter δ_{lab} , S is similar to the convection-only case. As given by *Vancoppenolle et al.* [2007], the reduced value (δ_{mod}) slightly improves the results.

[54] To conclude this section, we discuss the impact of the bottom boundary condition S_b (see equation (15)) on the simulated salinity profile. ν_b has historically been formulated as a function of ice growth rate ($\partial h_{i,b+}/\partial t$), following the empirical relationship of *Cox and Weeks* [1988], which gives values in the range $\sim 0.12\text{--}0.30$. This empirical theory has been successful in explaining the salinity and oxygen isotope profiles within the ice [*Weeks and Ackley*, 1986; *Souchez et al.*, 1987; *Eicken*, 1998]. *Weeks and Ackley* have shown that salt fractionation at the basal interface can be derived by approximating an advection-diffusion equation in the ice-ocean boundary layer. However, the concept of salt fractionation is not an accurate representation of the interface as *Notz and Worster* [2008]’s observation show a continuous transition in both salinity and liquid fraction at the ice-ocean interface. Here, the impact of basal boundary condition was tested in the model by running two simulations. In the first one (run 07 in Table 2), it was assumed that salt fractionation takes place

during ice formation at the base. In other words, the formula of *Cox and Weeks* [1988] was used to compute ν_b . In the control run (run 01 in Table 2), a continuous interface is assumed instead, and hence $\nu_b = 1$ was prescribed. Results show that the simulated salinity profile, in particular near the ice base, is not sensitive to the value of ν_b (see Figure 8). This is true because a sufficiently high value of D_σ^{tur} was used. In the $\nu_b = 1$ case, the newly created ice is more saline than if the interactive ν_b is used. Convection is also stronger hence new ice desalinates faster. Both processes cancel out, which is why the salinity of basal ice is not sensitive to ν_b .

5.2.3. Salt Fluxes

[55] We also investigate ice-ocean salt fluxes. In Table 3, the mean values of F^s for some of the sensitivity experiments and from the laboratory experiments of WO83 are shown. Time series from the control run are plotted in Figure 10. Since ice growth rates from WO83 are larger ($0.8\text{--}13\text{ cm d}^{-1}$) than our mean simulated value (0.4 cm d^{-1}), we extrapolated the measurements (using Figures 11 and 12 of WO83).

[56] Analysis highlights the following. First, F^s depends on the model representation of brine drainage. In runs CTL, DTUR_N1, CW, and NCW, the simulated values of F^s have the correct order of magnitude, $\sim 10^{-6}\text{ kg NaCl m s}^{-1}$, but are underestimated by a factor two. In DMOL_N1, F^s is underestimated by one order of magnitude. In contrast, the simulated salt flux does not change if one assumes that the ice-ocean salt flux is due to brine drainage only ($\nu_b = 1$) or due to both brine drainage and basal salt fractionation (ν_b as computed using formula of *Cox and Weeks* [1988]). Finally, in all experiments, even if $\nu_b = 1$, the ice growth rate and the ice-ocean salt flux are highly correlated (c.c. ~ 0.9) during the ice growth period.

[57] In spring, intense convective events are characterized by large salt fluxes (more than $3 \times 10^{-6}\text{ kg NaCl m s}^{-1}$). In summer, flushing events induce salt fluxes within $1\text{--}3 \times 10^{-6}\text{ kg NaCl m s}^{-1}$.

5.3. Winter-Spring Dynamics: Role of Surface Seawater Flooding

[58] In September, snow becomes deep enough for significant snow ice formation to occur in the model. At the same time, the ice growth rate is relatively low due to the insulating effect of deeper snow. Significant amounts of seawater flood the snow cover and load the upper ice layers with salt, which tends to increase the ice salinity at the vicinity of snow-ice interface. Concomitantly, due to the passage of warmer air masses, the upper ice temperature occasionally increases to values above -5°C . Relatively high values of salinity and temperature near the ice surface induce larger brine volume and porosities, which increases

Table 3. Simulated Salt Flux and Ice Growth Rate Averaged Over the Basal Ice Growth Period, 14 March to 10 October, for Several Sensitivity Experiments^a

	CTL	DTUR N1	DMOL N1	NCW	CW MOD	WO83
F^s	1.17	1.30	0.19	1.18	1.25	~ 2.5
$\partial h_{i,b+}/\partial t$	0.36	0.35	0.40	0.38	0.37	

^aSimulated salt flux is F^s ($10^{-6}\text{ kgNaClm}^{-2}\text{ s}^{-1}$), and ice growth rate is $\partial h_{i,b+}/\partial t$ (cm d^{-1}). For comparison, data of WO83, extrapolated using simulated growth rate of 0.4 cm d^{-1} , are shown.

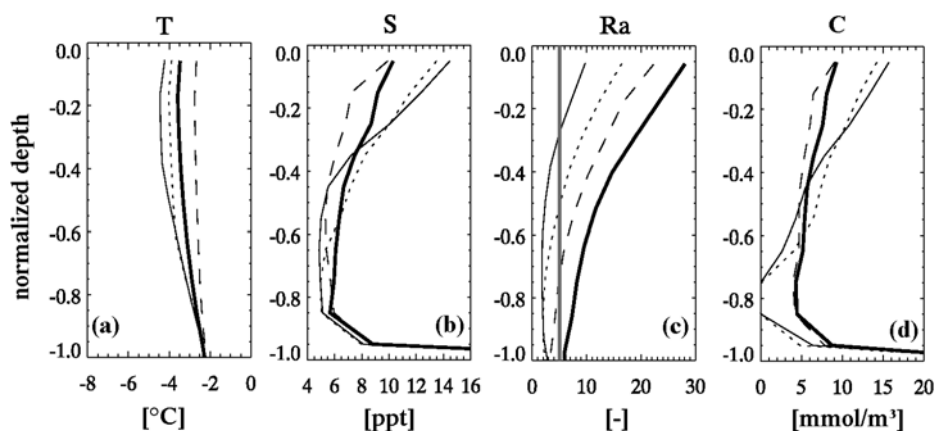


Figure 9. Normalized vertical profiles of (a) T , (b) S , (c) Ra , and (d) C in sea ice before, at the time of, and after a typical convective event, which occurs in run 2SNOW and has its maximal activity on 1 October. Dates: 17 September (solid thin curve), 24 September (dotted curve), 1 October (solid thick curve), and 8 October (dashed curve).

Ra near the ice surface. When Ra becomes supercritical over the whole ice column, intense convective events start.

[59] Convective events usually last one day in the model, but in some cases, a few successive events take place. They are quite sensitive to snowfall rate: in run CTL, there is one convective event (Oct 24), while in the run 2SNOW, there are eight of them. Such convective events have been observed within the Antarctic sea ice pack during Ice Station Weddell [Lytle and Ackley, 1996] and also during ISB [Tison *et al.*, 2007]. Those were suggested to initiate a vertical exchange of nutrient-poor brine with nutrient-rich seawater, enabling intense primary production [Fritsen *et al.*, 1994]. In Figure 9, the effect of one of those convective events on S , T , Ra , and C is shown. Convective events enable not only to evacuate salt but also to replenish nutrients through the interconnected brine network in a very efficient way. For instance, the convection associated with a simulated convective event around 1 October allows the DSi concentration to recover to around $4 \text{ mmol DSi m}^{-3}$ in the lower third of the ice where DSi was depleted.

[60] Convective events are accompanied by ice-ocean salt fluxes about one order of magnitude larger than average (see Figure 10). Only the Rayleigh number formulation of brine motion enables to capture such convective events. In Figure 10 (right), it can be seen that if the parameterization of Cox and Weeks [1988] is used, much more salt is kept near the surface in run 2SNOW and no intensification of the salt flux is simulated.

[61] The sensitivity of convective events to snowfall stresses the importance of surface entrainment of salt triggered by snow ice formation. There are uncertainties in the source of saline water near the surface associated with snow ice formation as explained by Maksym and Jeffries [2000]. Salty water may either come from lateral penetration of seawater through thermal cracks, leads, and ridges or from an upward flow of brine from the sea ice brine network toward the snow cover to maintain hydrostatic equilibrium. Those questions are beyond the scope of this paper. Nevertheless, the simulation shows that the model is able to intensify brine drainage and nutrient flow if there is a source of salt at the surface.

5.4. Biophysical Interactions

[62] All of the oceanic DSi is assumed to be initially trapped into new ice and then rejected by different means. In the absence of biochemical processes (i.e., algal uptake in the present simulations), the nutrient fluxes readily follow the salt fluxes. Primary production, consuming nutrients, reduces the brine concentration of DSi (ζ^{DSi}) and thus increases the gradient of C_{DSi} between ice and ocean, which in turn enhances the nutrient fluxes. Hence, there are potential biophysical interactions between algal uptake (biochemical process) and nutrient flux (physical process) which could be significant. In order to quantify the latter, we analyze the simulated nutrient budget in sea ice in CTL (algal uptake off) and CTL_BIO (algal uptake on) and do the same with a doubled snowfall rate.

[63] In Table 4, the components of the DSi budget are detailed for CTL, CTL_BIO, 2SNOW, and 2SNOW_BIO. Without algal uptake, the increase in DSi content is equal to the sum of the physical contributions: uptake (B , SI) and brine drainage (BD). In this abiotic case, in the run with normal (doubled) snowfall rate, the ice retains 20 (35)% of the DSi initially present in seawater (B). Therefore, in

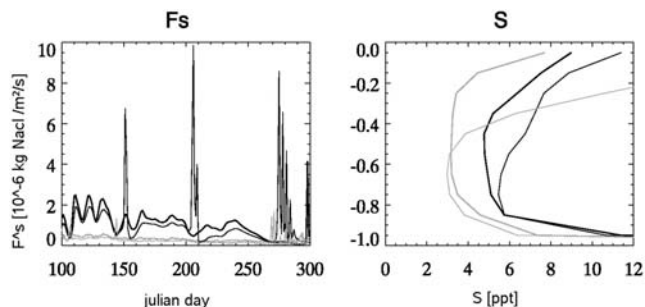


Figure 10. Time series of (left) salt flux (F_s) and (right) mean vertical salinity (S) profile between 9 April and 26 October. Different experiments are depicted: experiments CTL (thick black curve), CW_MOD (thick gray curve), 2SNOW (thin black curve), and 2SNOW_CW (thin gray curve).

Table 4. DSi Budget From Several Sensitivity Experiments During the Continuous Ice Growth Period, 14 March to 13 November^a

Experiment Name	$[M^{DSi}]_0^{t_1}$	$B + SI + BD$	B	SI	BD	β
CTL	6.3	6.3	30.2	2.2	-26.1	0
CTL_BIO	2.7	19.6	30.2	2.2	-12.8	-16.9
2SNOW	8.2	8.2	21.7	10.5	-23.9	0
2SNOW_BIO	4.9	25.1	21.7	10.5	-7.1	-20.2

^aSee Table 2 for description of sensitivity experiments. Sign convention assumes positive sign for a gain of DSi by the ice. B , SI, BD, and β are the contributions of basal congelation, snow ice formation, brine drainage, and biology, respectively. Units are mmol m^{-2} .

abiotic conditions, all the freshwater is stored in growing ice, while the majority of the DSi is rejected, which triggers a DSi accumulation in the upper ocean.

[64] Algal uptake decreases the concentration of nutrients dissolved in the brine (ζ^{DSi}), which affects the exchange of nutrients due to convection without modifying the strength of convection. In the simulations with active primary production (CTL_BIO and 2SNOW_BIO), the ice-ocean DSi exchange (F_{bd}^{DSi}) is reduced and may even reverse if $\zeta^{DSi} < \zeta_w^{DSi}$. In that case, the convective motion in the lowermost ice layers has two opposite effects: a salt rejection from and a DSi input to the ice. In turn, compared to the abiotic case, the nutrient content M^{DSi} is two to three times smaller with algal uptake. By contrast, in order to balance the algal sink, the total physical uptake of DSi by the ice ($B + SI + BD$) is three times larger. In the thin snow case (CTL_BIO), the total DSi remaining in the ice, either dissolved in brine (M^{DSi}) or consumed by algae (β), represents about 60% of the DSi initially present in seawater. In the thick snow case (2SNOW_BIO), because of intense convective events (see section 5.3), the sea ice DSi content is 115% of the DSi content of the seawater from which it formed. Therefore, nutrients are pumped from seawater to the ice to render it possible. Thus, in the case of sustained primary production, in contrast to salt, ice growth induces a decrease in nutrient concentration in the upper oceanic layers without import from below. Finally, in summer, from 13 November to 27 December, the total ice-ocean DSi flux associated with flushing is 5.2 (1.5) mmol DSi m^{-2} in the CTL (BIO) run.

6. Discussion

[65] Topics related to model validation, brine dynamics, convective events, and biophysical interactions are discussed in the first four parts of this section. In the last part, we synthesize the results using a simple box model.

6.1. Model Validation

[66] The simulated profiles of S are in quantitative agreement with observations. For DSi, the accord is only qualitative, which is due to the simplicity of the biological component. The largest concentration of nutrients simulated by the model is found near the ice surface and near its base. This has been identified to be associated with snow ice formation and to brine convection, respectively, and is in good agreement with typical observed locations of algae communities [Ackley and Sullivan, 1994]. In addition, the parameterization of convection enables the simulation of intense convective events, refilling nutrients stocks, similar

to the ones reported by Lytle and Ackley [1996] and recently observed during the ISB drift station.

6.2. Brine Dynamics in Growing Ice

[67] Sensitivity experiments illustrate that Ra -controlled convection in growing ice is able to represent *gravity drainage*. In any case, molecular diffusion is far too weak to explain the required desalination rates and the ice-ocean salt fluxes. Although some model tuning had to be done, the choice of the parameters Ra_c and D_σ^{tur} is not arbitrary. First, Notz and Worster [2008] observed in natural sea ice that values of Ra around 10 were associated with the highest desalination rates which they attributed to convection in the lowest few centimeters of ice. Such a high value arises in our model simulations as simulated for $Ra_c = 5$. Second, the salt turbulent diffusivities used in physical oceanography are usually several orders of magnitude larger than molecular diffusivities.

[68] We follow Weeks and Ackley [1986], who interpret the fractionation of salt near the ice base as due to convection. The model is not sensitive to ν_b (the basal salt fractionation coefficient) if gravity drainage is represented by convection. In the $\nu_b = 1$ case, all oceanic salt is accumulated in the ice during formation. However, since the ice salinity near the base is higher in that case than if a lower ν_b is used, the porosity and Rayleigh number are larger and hence convection is stronger, which enhances salt rejection. In other words, convection and salt fractionation have the same effect on ice salinity. However, the fractionation model is not suitable for biogeochemical species, which are affected by external sources and sinks interacting with convection.

6.3. Intense Convective Events

[69] The model simulates intense convective events associated with deep snow cover and mild air temperatures typical of spring that trigger supercritical Rayleigh number over the entire brine column. Convective events following seawater flooding strongly affect salt and nutrients. Seawater flooding seems particularly important as it also leads either to snow ice or to gap layer formation [e.g., Ackley et al., 2008]. However, numerous uncertainties remain. First, the pathways of brine and/or seawater during surface flooding are uncertain. In addition, measurements of permeability (a key parameter in flooding events) are missing for highly saline Antarctic sea ice. Finally, the role of heat transfer associated with brine motion during those convective events was neglected and should be investigated.

6.4. Biophysical Interactions

[70] In our model, algal uptake interacts with the physics in a way that intensifies upward fluxes of DSi. This suggests a new understanding of the dynamics of impurities in the vicinity of the ice-ocean interface (see Figure 11). Convective mixing of saline brine with seawater desalinates the ice and replenishes nutrients by mixing nutrient-poor brine with nutrient-rich seawater. In other words, convection induces an *apparent* salt fractionation and pumps nutrients in the ice, which reduces the nutrient limitation near the ice base. Two meteorological situations seem particularly favorable for nutrient replenishment in the ice. First, cold air temperatures promote ice growth and brine convection near the ice

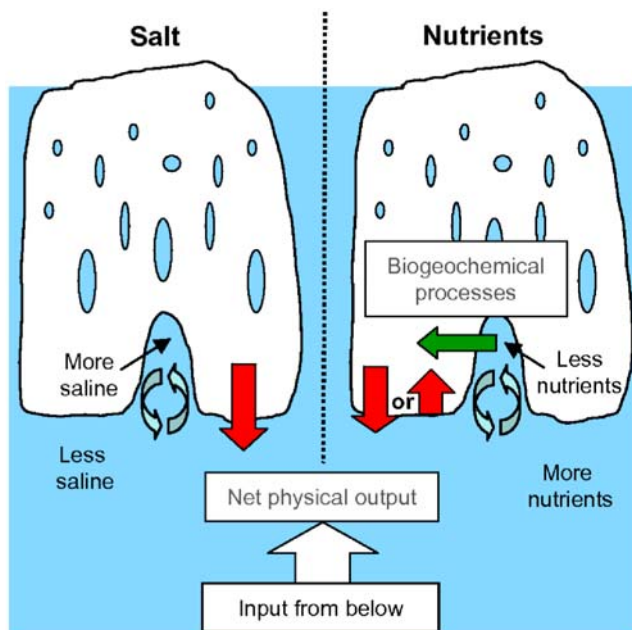


Figure 11. Sketch of (left) salt and (right) nutrient exchanges at the ice-ocean interface proposed in this paper. Salt remains embedded in sea ice during its formation, dissolved within the liquid phase. Salt is then rejected to the ocean through convective mixing of relatively saline brine with relatively less saline seawater. This results in a net concentration of salt in the upper oceanic layer. Similarly, dissolved nutrients remain embedded in sea ice during formation. However, in contrast to salt, biological or chemical processes deplete the concentration of nutrients in the liquid phase, which reduces nutrient export to the ocean or even induces upward nutrient fluxes by mixing of nutrient-rich seawater with nutrient-depleted brine by convection. This leads to nutrient replenishment within the ice and may reduce the nutrient concentration in the upper oceanic layer.

base. Second, snowfall, if large enough, may lead to convective instabilities throughout the whole sea ice column. In summer, if surface meltwater is produced, flushing occurs and nutrients are expelled from the ice cover.

[71] The role of snow in the Southern Ocean is in apparent contradiction with the Arctic. In the Southern Ocean, deep snow intensifies nutrient supply through seawater flooding. For instance, based on Antarctic sea ice samples at ISB (Liège site), [Dumont, 2009] found higher Chla concentrations under deep snow than under thin snow, due to seawater flooding. In the Arctic, ice is thicker and spring air temperatures are colder. Hence, deep snow does not trigger intense convective events and does not intensify nutrient supply near the surface. As a result, in the Arctic, deep snow cover reduces light input near the ice base, which leads to relatively low Chla concentrations [see, e.g., Mundy *et al.*, 2005].

6.5. A Simple Box Model to Illustrate Biophysical Interactions in Sea Ice

[72] In order to illustrate the essence of the biophysical pump, we use a simple box model. For any biochemical

tracer characterized by a concentration in brine ζ , biological sinks tend to decrease ζ . This increases the seawater-brine gradient of ζ and the associated convective flux and then replenishes brine with dissolved material. Efficiency of convective mixing will be maximal in the limit $\zeta \rightarrow 0$, i.e., for maximal brine-seawater ζ gradient. This limit is reached when the biochemical sink is strong enough to deplete the liquid phase of dissolved material.

[73] The efficiency of the biophysical pump is controlled by the ratio of two time scales, associated with biological uptake and convection time scales. Let us assume that exchanges of dissolved material are confined to a basal permeable layer of thickness $H = 5$ cm and characterized by a convective flux (F) and by an external (biological) sink (S_β), respectively, providing material to and removing it from the liquid phase. In this framework, ζ follows:

$$e \frac{d\zeta}{dt} = -S_\beta + \frac{F}{H}, \quad (28)$$

where F is given by

$$F = -\frac{De}{2} \left(\frac{\zeta - C_w}{H} \right). \quad (29)$$

In the above equation, $D \sim 10^{-6}$ m²/s is a turbulent diffusivity, $e \sim 30\%$ is the mean relative brine volume in the permeable layer, and C_w refers to the concentration of dissolved material in seawater. Combining equations (28) and (29), one obtains

$$e \frac{d\zeta}{dt} = -S_\beta + \frac{De}{2} \left(\frac{C_w - \zeta}{H^2} \right). \quad (30)$$

The solution of (30) has two components. The first one is an exponential term decreasing with time and the second one represents the equilibrium solution prevailing after some time:

$$\zeta_{eq} = C_w \left(1 - \frac{T_\phi}{T_\beta} \right). \quad (31)$$

Here, $T_\beta = C_w/S_\beta$ and $T_\phi = 2H^2/De$ are the time scales associated with the biological and physical processes, respectively. Using the aforementioned values of H , D , and e , one gets $T_\phi \sim 1.6 \times 10^4$ s. It is shown in equation (31) that the efficiency of the biological pump will be large if the ratio T_ϕ/T_β is not negligible, i.e., if biological processes are relatively quick compared to convection.

[74] For salt, there is no biological sink, i.e., T_β is infinite and the efficiency of the pump is zero. Convection always acts to reject salt from the ice: there is apparent *salt-fractionation* at the ice-ocean interface. For DSI in the Weddell Sea, assuming that algal uptake is given by equation (22), $T_\beta \sim 10^7$ s, the ratio T_ϕ/T_β is $\sim 10^{-3}$, and the efficiency of the pump is far from its maximum. This suggests that algae would be hardly nutrient-limited under growing ice conditions in the lower permeable regions of the ice cover. Upper in the ice (except near the surface), algae would easily be nutrient limited due to reduced permeability and restricted material exchanges.

[75] In reality, biophysical interactions of this kind still hold except that the biological processes are far more complex. An extreme case for which the pump is highly efficient may well be provided by iron. Iron concentrations in Antarctic sea ice have been reported to be one to two orders of magnitude larger than in seawater below [Lannuzel *et al.*, 2007, 2008]. This has been found contradictory compared to other impurities such as salt or nutrients. Our results suggest that this contradiction is resolved if there exists biological or chemical sinks (such as adsorption of iron on surfaces of brine inclusions or on organic matter) that are associated with time scales small enough compared to the time scale of brine convection. If so, those biochemical processes could take advantage of the powerful convective pump, which may explain the large iron concentrations in Antarctic sea ice. This will be investigated in future studies.

7. Conclusions

[76] In this paper, a one-dimensional biophysical sea ice model was used to test whether brine drainage can account for nutrient supply. To accomplish this goal, a new representation of salt and nutrients in sea ice, based on convection-diffusion equations, was developed and tested. The biological component of the model was kept deliberately simple. The results presented here correspond to an ideal situation in which one nutrient (DSi) is consumed at a constant rate by algae growing at a constant rate when exposed to light. The model was set up to simulate dissolved silica in first-year Antarctic pack ice.

[77] The model simulates the sea ice mass balance, salinity, and DSi vertical profiles as well as the ice-ocean salt fluxes in qualitative agreement with observations. In winter, brine convection in the lowermost 5–10 cm of ice explains both winter sea ice desalination rates and nutrient replenishment. Flooding of the basal snow cover by seawater in spring also contributes to the DSi input to the ice. Intense convective events promoted by deep snow cover in late spring significantly enhance the supply of DSi. Summer meltwater percolation may, if present, flush nutrients away from the ice. Finally, there are important biophysical interactions between convection and biochemical processes that significantly affect the ice-ocean DSi fluxes.

[78] The framework proposed here to model salt and nutrients is one necessary step toward more realistic biophysical sea ice models. However, more experimental and theoretical work is needed to improve the models. Critical topics are the links between permeability and porosity, thermal equilibrium, and the links between turbulent diffusivities and the Rayleigh number, as they were shown to significantly affect the simulated profiles of ice salinity and nutrients. In addition, for realistic simulations, the model presented here obviously lacks a realistic representation of the biological processes [e.g., Arrigo *et al.*, 1993; Lavoie *et al.*, 2005; Nishi and Tabet, 2007; Pasquer *et al.*, 2005], which should be improved in future model versions.

[79] **Acknowledgments.** Martin Vancoppenolle and Hugues Goosse are supported by FNRS. Steve Ackley, Chris Fritsen, Katia Groznaia, and members of the Sea ice Biogeochemistry in a changing CLIMate (SIBCLIM) and Assessing the sensitivity of the Southern Ocean's biological carbon pump to climate change (BELCANTO) communities as well as

SIMBA-IPY cruise participants and staff are acknowledged for discussions. The two Referees and Editor are gratefully acknowledged for careful review of the manuscript. This work was done within the framework of the project BELCANTO (funded by the Belgian Science Federal Policy Office).

References

- Ackley, S. F., and C. W. Sullivan (1994), Physical controls on the development and characteristics of Antarctic sea ice biological communities: A review and synthesis, *Deep Sea Res., Part 1*, *41*, 1583–1604.
- Ackley, S. F., M. Lewis, C. Fritsen, and H. Xie (2008), Internal melting in Antarctic sea ice: Development of “gap layers”, *Geophys. Res. Lett.*, *35*, L11503, doi:10.1029/2008GL033644.
- Arrigo, K. R., J. N. Kremer, and C. W. Sullivan (1993), A simulated Antarctic fast ice ecosystem, *J. Geophys. Res.*, *98*, 6929–6946.
- Assur, A. (1958), Composition of sea ice and its tensile strength, in *Arctic Sea Ice*, pp. 106–138, U.S. Natl. Acad. Sci., Washington, D. C.
- Bitz, C. M., and W. H. Lipscomb (1999), An energy-conserving thermodynamic model of sea ice, *J. Geophys. Res.*, *104*, 15,669–15,677.
- Clarke, D. B., and S. F. Ackley (1984), Sea ice structure and biological activity in the Antarctic marginal ice zone, *J. Geophys. Res.*, *89*, 2087–2095.
- Conkright, M. E., R. A. Locarnini, H. E. Garcia, T. D. O'Brien, T. P. Boyer, C. Stephens, and J. L. J. I. Antonov (2001), World Ocean Atlas 2001: Objective analyses, data statistics and figures, Internal Rep. 17, 17 pp., NOAA, Silver Spring, Md.
- Cota, G. F., S. J. Prinsenberg, E. B. Bennett, J. W. Loder, M. R. Lewis, J. L. Anning, N. H. F. Watson, and L. R. Harris (1987), Nutrient flux during extended blooms of arctic ice algae, *J. Geophys. Res.*, *92*, 1951–1962.
- Cox, G. F. N., and W. F. Weeks (1975), Brine drainage and initial salt entrapment in sodium chloride ice, *CRREL Res. Rep. 345*, U. S. Army Cold Reg. Res. and Eng. Lab., Hanover, N. H.
- Cox, G. F. N., and W. F. Weeks (1988), Numerical simulations of the profile properties of undeformed first-year sea ice during growth season, *J. Geophys. Res.*, *93*, 12,449–12,460.
- Delille, B. (2006), Inorganic carbon dynamics and air-ice-sea CO₂ fluxes in the open and coastal waters of the Southern Ocean, Ph.D. thesis, Univ. de Liège, Liège, Belgium.
- Dieckmann, G. S., M. A. Lange, S. F. Ackley, and J. C. Jennings (1991), Nutrient status in sea ice of the Weddell Sea during winter: Effects of sea ice texture and algae, *Polar Biol.*, *11*, 449–456.
- Dumont, I. (2009), Interactions between the microbial network and the organic matter in the Southern Ocean: Impacts on the biological carbon pump, Ph.D. thesis, Univ. Libre de Bruxelles, Brussels.
- Eicken, H. (1992), Salinity profiles of Antarctic sea ice: Field data and model results, *J. Geophys. Res.*, *97*, 15,545–15,557.
- Eicken, H. (1998), Factors determining microstructure, salinity and stable-isotope composition of Antarctic sea ice: Deriving modes and rates of ice growth in the Weddell sea from microstructural, salinity and stable-isotope data, in *Antarctic Sea Ice: Physical Processes, Interactions and Variability*, *Antarct. Res. Ser.*, vol. 74, edited by M. O. Jeffries, pp. 89–122, AGU, Washington, D. C.
- Eicken, H., M. A. Lange, and G. S. Dieckmann (1991), Spatial variability of sea ice properties in the northwestern Weddell Sea, *J. Geophys. Res.*, *96*, 10,603–10,615.
- Eicken, H., H. R. Krouse, D. Kadko, and D. K. Perovich (2002), Tracer studies of pathways and rates of meltwater transport through arctic summer sea ice, *J. Geophys. Res.*, *107*(C10), 8046, doi:10.1029/2000JC000583.
- Eide, L., and S. Martin (1975), The formation of brine drainage features in young sea ice, *J. Glaciol.*, *14*, 137–154.
- Freitag, J. (1999), Untersuchungen zur hydrologie des arktischen meereises: konsequenzen für den kleinskaligen stofftransport (in German), *Ber. Polarforsch.*, *325*, 150 pp.
- Fripiat, F., D. Cardinal, J.-L. Tison, A. Worby, and L. André (2007), Diatom-induced silicon isotopic fractionation in antarctic sea ice-atmosphere, *J. Geophys. Res.*, *112*, G02001, doi:10.1029/2006JG000244.
- Fritsen, C., V. Lytle, S. Ackley, and C. Sullivan (1994), Autumn bloom of Antarctic pack-ice algae, *Science*, *266*, 782–784.
- Fritsen, C., S. Ackley, J. Kremer, and C. Sullivan (1998), Flood-freeze cycles and microalgal dynamics in Antarctic pack ice, in *Antarctic Sea Ice: Biological Processes, Interactions, and Variability*, *Antarct. Res. Ser.*, vol. 73, edited by M. P. Lizotte and K. R. Arrigo, pp. 1–21, AGU, Washington, D. C.
- Giannelli, V., D. N. Thomas, C. Haas, G. Kattner, H. Kennedy, and G. S. Dieckmann (2001), Behaviour of dissolved organic matter and inorganic nutrients during experimental sea-ice formation, *Ann. Glaciol.*, *33*, 317–321.
- Golden, K. M., S. F. Ackley, and V. I. Lytle (1998), The percolation phase transition in sea ice, *Science*, *282*, 2238–2241.
- Golden, K., H. Eicken, A. L. Heaton, J. Miner, D. J. Pringle, and J. Zhu (2007), Thermal evolution of permeability and microstructure in sea ice, *Geophys. Res. Lett.*, *34*, L16501, doi:10.1029/2007GL030447.

- Goosse, H. (1997), Modeling the large-scale behavior of the coupled ocean–sea ice system, Ph.D. thesis, Univ. Catholique de Louvain, Louvain-la-Neuve, Belgium.
- Gow, A. J., S. F. Ackley, K. R. Buck, and K. M. Golden (1987), Physical and structural characteristics of Weddell sea pack ice, *CRREL Rep. 87-14*, U.S. Army Cold Reg. Res. and Eng. Lab., Hanover, N. H.
- Grenfell, T. C., and G. A. Maykut (1977), The optical properties of ice and snow in the Arctic basin, *J. Glaciol.*, *18*, 445–463.
- Grenfell, T. C., B. Light, and D. K. Perovich (2006), Spectral transmission and implications for the partitioning of shortwave radiation in Arctic sea ice, *Ann. Glaciol.*, *44*, 1–6.
- Haas, C., M. Nicolaus, S. Willmes, A. P. Worby, and D. Flinspach (2008), Sea ice and snow thickness and physical properties of an ice floe in the western Weddell Sea and their changes during spring warming, *Deep Sea Res., Part II*, *55*, 963–974, doi:10.1016/j.dsr2.2007.12.020.
- Holland, M. M., C. M. Bitz, E. C. Hunke, W. H. Lipscomb, and J. Schramm (2006), Influence of the sea ice thickness distribution on polar climate in CCSM3, *J. Clim.*, *19*, 2398–2414.
- Hunke, E. C., and W. H. Lipscomb (2004), CICE: The Los Alamos sea ice model documentation and software user's manual, *Tech. Rep. LA-CC-98-16*, Los Alamos Natl. Lab., Los Alamos, N. M.
- Jeffries, M. O., R. A. Shaw, K. Morris, A. L. Veazey, and H. R. Krouse (1994), Crystal structure, stable isotopes ($\delta^{18}\text{O}$), and development of sea ice in the Raoss, Amundsen and Bellingshausen seas, Antarctica, *J. Geophys. Res.*, *99*, 985–995.
- Jeffries, M., A. Worby, K. Morris, and W. F. Weeks (1997), Seasonal variations in the properties and structural composition of sea ice and snow cover in the Bellingshausen and Amundsen sea, Antarctica, *J. Glaciol.*, *43*, 138–151.
- Kalnay, E., et al. (1996), The NCEP/NCAR 40-year reanalysis project, *Bull. Am. Meteorol. Soc.*, *77*, 437–471.
- Kottmeier, S. T., and C. W. Sullivan (1987), Late winter primary production and bacterial production in sea ice and seawater west of the Antarctic peninsula, *Mar. Ecol. Prog. Ser.*, *36*, 287–298.
- Krembs, C., H. Eicken, K. Junge, and J. W. Deming (2002), High concentrations of exopolymeric substances in Arctic winter sea ice: Implications for the polar ocean carbon cycle and cryoprotection of diatoms, *Deep Sea Res., Part I*, *49*, 2163–2181, doi:10.1016/S0967-0637(02)00122-X.
- Lancelot, C., A. de Montety, H. Goosse, S. Becquevort, V. Schoemann, B. Pasquer, and M. Vancoppenolle (2009), Spatial distribution of the iron supply to phytoplankton in the Southern Ocean: A model study, *Biogeosci. Discuss.*, *6*, 4919–4962.
- Lange, M., and H. Eicken (1991), The sea ice thickness distribution in the northwestern Weddell Sea, *J. Geophys. Res.*, *96*, 4821–4837.
- Lannuzel, D., V. Schoemann, J. de Jong, J.-L. Tison, and L. Chou (2007), Distribution and biogeochemical behaviour of iron in the east Antarctic sea ice, *Mar. Chem.*, *106*, 18–32, doi:10.1016/j.marchem.2006.06.010.
- Lannuzel, D., V. Schoemann, J. de Jong, L. Chou, B. Delille, S. Becquevort, and J.-L. Tison (2008), Iron study during a time series in the western Weddell pack ice, *Mar. Chem.*, *108*, 85–95, doi:10.1016/j.marchem.2007.10.006.
- Lavoie, D., K. Denman, and C. Michel (2005), Modeling ice algal growth and decline in a seasonally ice-covered region of the Arctic (Resolute Passage, Canadian archipelago), *J. Geophys. Res.*, *110*, C11009, doi:10.1029/2005JC002922.
- Light, B., G. A. Maykut, and T. C. Grenfell (2003), Effects of temperature on the microstructure of first-year Arctic sea ice, *J. Geophys. Res.*, *108*(C2), 3051, doi:10.1029/2001JC000887.
- Light, B., T. C. Grenfell, and D. K. Perovich (2008), Transmission and absorption of solar radiation by Arctic sea ice during the melt season, *J. Geophys. Res.*, *113*, C03023, doi:10.1029/2006JC003977.
- Lizotte, M. P. (2003), The microbiology of sea ice, in *Sea Ice: An Introduction to Its Physics, Chemistry, Biology and Geology*, edited by D. N. Thomas and G. S. Dieckmann, pp. 184–210, Blackwell, Malden, Mass.
- Lytle, V., and S. Ackley (1996), Heat flux through sea ice in the western Weddell sea: Convective and conductive transfer processes, *J. Geophys. Res.*, *101*, 8853–8868.
- Maksym, T., and M. O. Jeffries (2000), A one-dimensional percolation model of flooding and snow ice formation on Antarctic sea ice, *J. Geophys. Res.*, *105*, 26,313–26,331.
- Maksym, T., and T. Markus (2008), Antarctic sea ice thickness and snow-to-ice conversion from atmospheric reanalysis and passive microwave snow depth, *J. Geophys. Res.*, *113*, C02S12, doi:10.1029/2006JC004085.
- Massom, R. A., et al. (2001), Snow on Antarctic sea ice, *Rev. Geophys.*, *39*, 413–445.
- Maykut, G. A., and N. Untersteiner (1971), Some results from a time-dependent thermodynamic model of sea ice, *J. Geophys. Res.*, *76*, 1550–1575.
- Mundy, C., D. Barber, and C. Michel (2005), Variability of thermal, physical and optical properties pertinent to sea ice algae biomass during spring, *J. Mar. Syst.*, *58*, 107–120, doi:10.1016/j.jmarsys.2005.07.003.
- Nakawo, M., and N. K. Sinha (1981), Growth rate and salinity profile of first-year sea ice in the high Arctic, *J. Glaciol.*, *27*, 315–331.
- Nicolaus, M., C. Haas, J. Bareiss, and S. Willmes (2006), A model study of differences of snow thinning on Arctic and Antarctic first-year sea ice during spring and summer, *Ann. Glaciol.*, *44*, 147–153.
- Niedrauer, T. M., and S. Martin (1979), An experimental study of brine drainage and convection in young sea ice, *J. Geophys. Res.*, *84*, 1176–1186.
- Nishi, Y., and S. Tabeta (2007), Sunlight and tidal interaction as a mechanism of carbon transport in an ice-covered region: Results of a coupled ice-ocean ecosystem model, *Cont. Shelf Res.*, *27*, 1–19, doi:10.1016/j.csr.2006.08.005.
- Nishi, Y., and S. Tabeta (2008), Relation of material exchange between sea ice and water to a coupled ice-ocean ecosystem at the Hokkaido coastal region of the Okhotsk sea ice, *J. Geophys. Res.*, *113*, C01003, doi:10.1029/2006JC004077.
- Notz, D., and M. G. Worster (2006), A one-dimensional enthalpy model of sea ice, *Ann. Glaciol.*, *44*, 123–128.
- Notz, D., and M. G. Worster (2008), In situ measurements of the evolution of young sea ice, *J. Geophys. Res.*, *113*, C03001, doi:10.1029/2007JC004333.
- Notz, D., and M. G. Worster (2009), Desalination processes in sea ice, *J. Geophys. Res.*, *114*, C05006, doi:10.1029/2008JC004885.
- Notz, D., J. S. Wettlaufer, and M. G. Worster (2005), A non-destructive method for measuring the salinity and solid fraction of growing sea ice in situ, *J. Glaciol.*, *51*, 159–166.
- Pasquer, B., G. Laruelle, S. Becquevort, V. Schoemann, H. Goosse, and C. Lancelot (2005), Linking ocean biogeochemical cycles and ecosystem structure and function: Results of the complex SWAMCO-4 model, *J. Sea Res.*, *53*(1–2), 93–108.
- Pringle, D. J., H. Eicken, H. J. Trodahl, and L. Backstrom (2007), Thermal conductivity of landfast Antarctic and Arctic sea ice, *J. Geophys. Res.*, *112*, C04017, doi:10.1029/2006JC003641.
- Reeburgh, W. S. (1984), Fluxes associated with brine motion in growing sea ice–atmosphere, *Polar Biol.*, *3*, 29–33.
- Sarthou, G., K. R. Timmermans, S. Blain, and P. Tréguer (2005), Growth physiology and fate of diatoms in the ocean: A review, *J. Sea Res.*, *53*, 25–42.
- Schmidt, G., C. M. Bitz, U. Mikolajewicz, and L.-B. Tremblay (2004), Ice–ocean boundary conditions for coupled models, *Ocean Modell.*, *7*, 59–74, doi:10.1016/S1463-5003(03)00030-1.
- Schwerdtfeger, P. (1963), The thermal properties of sea ice, *J. Glaciol.*, *4*, 789–807.
- Semiletov, I., A. Makshtas, and S. Akasofu (2004), Atmospheric CO₂ balance: The role of Arctic sea ice, *Geophys. Res. Lett.*, *31*, L05121, doi:10.1029/2003GL017996.
- Serreze, M., M. Holland, and J. Stroeve (2007), Perspectives on the Arctic's shrinking sea-ice cover, *Science*, *315*, 1533–1536, doi:10.1126/science.1139426.
- Souchez, R., J.-L. Tison, and J. Jouzel (1987), Freezing rate determination by the isotopic composition of the ice, *Geophys. Res. Lett.*, *4*, 599–602.
- Thomas, D. N., and G. S. Dieckmann (Eds.) (2003), *Sea Ice: An Introduction to Its Physics, Chemistry, Biology and Geology*, Blackwell, Malden, Mass.
- Thomas, D. N., and S. Papadimitriou (2003), Biogeochemistry of sea ice, in *Sea Ice: An Introduction to Its Physics, Chemistry, Biology and Geology*, pp. 267–302, Blackwell, Malden, Mass.
- Tison, J.-L., B. Delille, J. de Jong, M. Vancoppenolle, I. Dumont, F. Masson, F. Brabant, N.-X. Geilfus, and G. Carnat (2007), Belgian contribution to the physical and biogeochemical investigations of sea ice and underlying seawater during the NB Palmer Simba Cruise (October 2007), Simba cruise report, Univ. Libre de Bruxelles, Brussels, Belgium.
- Tison, J.-L., A. P. Worby, B. Delille, F. Brabant, S. Papadimitriou, D. N. Thomas, J. de Jong, D. Lannuzel, and C. Haas (2008), Temporal evolution of decay summer first-year sea ice in the western Weddell sea, Antarctica, *Deep Sea Res., Part IIA*, *55*, 975–987, doi:10.1016/j.dsr2.2007.12.021.
- Untersteiner, N. (1968), Natural desalination and equilibrium salinity profile of perennial sea ice, *J. Geophys. Res.*, *73*, 1251–1257.
- Vancoppenolle, M., T. Fichefet, and C. M. Bitz (2006), Modeling the salinity profile of undeformed Arctic sea ice, *Geophys. Res. Lett.*, *33*, L21501, doi:10.1029/2006GL028342.
- Vancoppenolle, M., C. M. Bitz, and T. Fichefet (2007), Summer landfast sea ice desalination at point barrow: Model and observations, *J. Geophys. Res.*, *112*, C04022, doi:10.1029/2006JC003493.
- Vancoppenolle, M., T. Fichefet, H. Goosse, S. Bouillon, G. Madec, and M. M. Maqueda (2009a), Simulating the mass balance and salinity of Arctic and Antarctic sea ice. 1. Model description and validation, *Ocean Modell.*, *27*, 33–53, doi:10.1016/j.ocemod.2008.10.005.

- Vancoppenolle, M., T. Fichefet, and H. Goosse (2009b), Simulating the mass balance and salinity of Arctic and Antarctic sea ice. 2. Sensitivity to salinity processes, *Ocean Modell.*, 27, 54–69, doi:10.1016/j.ocemod.2008.11.003.
- Wakatsuchi, M., and N. Ono (1983), Measurements of salinity and volume of brine excluded from growing sea ice, *J. Geophys. Res.*, 88, 2943–2951.
- Weeks, W. F., and S. F. Ackley (1986), The growth, structure, and properties of sea ice, in *The Geophysics of Sea Ice, NATO ASI Ser., Ser. B*, vol. 146, pp. , 9–164, Plenum, New York.
- Worby, A. P., and R. A. Massom (1995), The structure and properties of sea ice and snow cover in east Antarctic pack ice-atmosphere, *Res. Rep. 7*, Antarct. CRC, Hobart, Tasmania, Australia.
- Worby, A. P., C. A. Geiger, M. J. Paget, M. L. V. Woert, S. F. Ackley, and T. L. DeLiberty (2008), The thickness distribution of Antarctic sea ice, *J. Geophys. Res.*, 113, C05S92, doi:10.1029/2007JC004254.
- Worster, M. G. (1992), The dynamics of mushy layers, in *Interactive Dynamics of Convection and Solidification*, pp. 113–138, Kluwer Acad., Norwell, Mass.
-
- A. de Montety, T. Fichefet, H. Goosse, and M. Vancoppenolle, Institut d’Astronomie et de Géophysique Georges Lemaitre, Université Catholique de Louvain, Chemin du Cyclotron, 2, B-1348 Louvain-la-Neuve, Belgium. (vancop@ast.ucl.ac.be)
- J.-L. Tison, Laboratoire de Glaciologie, Université Libre de Bruxelles, CP 160/03, Av. F.D. Roosevelt, 50, Bruxelles, B-1050 Belgium.
- B. Tremblay, Department of Atmospheric and Oceanic Sciences, McGill University, 805 Sherbrooke St. W., Montreal, QC H3A 2K6, Canada.